We are IntechOpen,
the world's leading publisher of
Open Access books
Built by scientists, for scientists

4,800
Open access books available

122,000
International authors and editors

135M
Downloads

Our authors are among the

154
Countries delivered to

TOP 1%
most cited scientists

12.2%
Contributors from top 500 universities

CLARIVATE ANALYTICS
BOOK CITATION INDEX
INDEXED

WEB OF SCIENCE™

Selection of our books indexed in the Book Citation Index
in Web of Science™ Core Collection (BKCI)

Interested in publishing with us?
Contact book.department@intechopen.com

Numbers displayed above are based on latest data collected.
For more information visit www.intechopen.com

Coupled Mode Theory of Photonic Crystal Lasers

Marcin Koba[1] and Pawel Szczepanski[2]
[1]*University of Warsaw, National Institute of Telecommunications*
[2]*Warsaw University of Technology, National Institute of Telecommunications*
Poland

1. Introduction

Photonic crystals (PC) are structures with periodic variation of the refractive index in one, two or three spatial dimensions. The dynamic development of experimental and theoretical work on photonic crystals has been launched by Yablonovitch (1987; 1993) and Sajeev John (1987) publications, although the idea of periodic structures had been known since Strutt (1887).

The main property of photonic crystal is the existence of a frequency range, for which the propagation of electromagnetic waves in the medium is not permitted. These frequency ranges are commonly known as photonic band gaps, giving the ability to modify the structure parameters, e.g. group velocity, coherence length, gain, and spontaneous emission. This type of periodic structures is used in both passive and active devices.

1.1 Two-dimensional photonic crystal lasers

Much of the research on active structures is devoted to efficient photonic sources of coherent radiation. Photonic crystals are one of these structures, and they are used in lasers as mirrors (Dunbar et al. (2005); Scherer et al. (2005)), active waveguides (Watanabe & Baba (2006)), coupled cavities (Steinberg & Boag (2006)), defect microcavities (Asano et al. (2006); Lee et al. (2004)), and the laser active region (Cojocaru et al. (2005)).

Lasers with defect two-dimensional photonic crystals are known for their high finesse (Monat et al. (2001)) and very low threshold (Nomura et al. (2008)).

Photonic crystal band-edge lasers allow to obtain edge (Cojocaru et al. (2005)) and surface emission (Turnbull et al. (2003); Vurgaftman & Meyer (2003)) of coherent light from large cavity area. They also allow to control the output beam pattern by manipulation of the primitive cell geometry (Iwahashi et al. (2010); Miyai et al. (2006)), provide low threshold (Susa (2001)), and beams which can be focused to a size less than the wavelength (Matsubara et al. (2008)).

The photonic crystal structures lasing wavelengths span from terahertz (Chassagneux et al. (2009); Sirigu et al. (2008)), through infrared (Kim et al. (2006)) to visible (Lu et al. (2008); Zhang et al. (2006)).

1.2 Radiation generation modeling in photonic crystal lasers

Laser action in photonic crystal structures has been theoretically studied and centered on the estimation of the output parameters (Czuma & Szczepanski (2005); Lesniewska-Matys et al. (2005)) and models describing light generation processes e.g. (Florescu et al. (2002); Koba, Szczepanski & Kossek (2011); Sakai et al. (2010)). The most sophisticated and general (it describes one-, two-, and three-dimensional structures) semiclassical model of light generation in photonic structures is presented in (Florescu et al. (2002)). Theoretical analysis of photonic crystal lasers based on two-dimensional plane wave expansion method (PWEM) (Imada et al. (2002); Sakai et al. (2005)) and finite difference time domain method (FDTD) (Imada et al. (2002); Noda & Yokoyama (2005)) confirm experimental results. Nevertheless these methods suffer from important disadvantages, i.e. plane wave method gives a good approximation for infinite structures, whereas finite difference time domain method is suited for structures with only a few periods and consumes huge computer resources for the analysis of real photonic structures. Therefore these methods are not very convenient for design and optimization of actual photonic crystal lasers. Hence, different, less complicated methods of analysis of two-dimensional photonic crystal lasers are developed. These methods are meant to effectively support the design process of such lasers. They are based on a coupled mode theory (Sakai et al. (2006); Vurgaftman & Meyer (2003)) and focused on square and triangular lattice photonic crystals (Koba & Szczepanski (2010); Koba, Szczepanski & Kossek (2011); Koba, Szczepanski & Osuch (2011); Sakai et al. (2007; 2010; 2008)).

The Sakai et al. (2007; 2010) works contain a mathematical description and numerical results of the threshold analysis of two-dimensional (2-D) square lattice photonic crystal laser with TM and TE polarization. They introduce general coupled mode relations for a threshold gain, a Bragg frequency deviation and field distributions, and give calculation results for some specific values of coupling coefficients. Additionally, in (Sakai et al. (2007)) the effect of boundary reflections has been investigated, and it has been shown that the mode properties can be adjusted by changing refractive index or boundary conditions.

In Sakai et al. (2008) paper, the analytical description of triangular lattice photonic crystal cavity for TE polarization has been given. In this work the analysis was focused on the coupled wave equations and the dependence of the resonant frequencies on the coupling coefficients.

In Sakai et al. (2007; 2010; 2008) works threshold analysis has been conducted for specific values of coupling coefficient and TM polarization for triangular has not been considered.

The equations for triangular lattice photonic crystal laser with TM polarization has been shown in Koba, Szczepanski & Kossek (2011), and the evaluation of these is shown in this chapter.

The mentioned semiclassical model, presented by Florescu et al. (2002) describing an above threshold analysis is complicated and difficult to implement. To overcome this drawback, this chapter also includes an overview of our works (Koba & Szczepanski (2010); Koba, Szczepanski & Kossek (2011); Koba, Szczepanski & Osuch (2011)), where we introduced easy to implement models for an above threshold analysis of a two-dimensional photonic crystal laser.

Therefore, in the subsequent parts of this chapter we addressed the issues of the laser threshold characteristics in the wide range of the coupling coefficient and described all four cases of square and triangular lattice photonic crystal structures with TE and TM polarization. We also describe an above threshold analysis for these structures.

Thus, in this chapter we will summon the analytical models of the threshold and above threshold light generation in photonic crystal band-edge lasers considering square and triangular lattice structures with TE and TM polarization. Theoretical evaluation in this chapter is based on coupled wave model and energy theorem.

2. Structure definition

This paper describes the two-dimensional photonic crystals which properties can be described by the complex relative electrical permittivity ε. The cross sections of these structures are shown schematically in Fig. 1
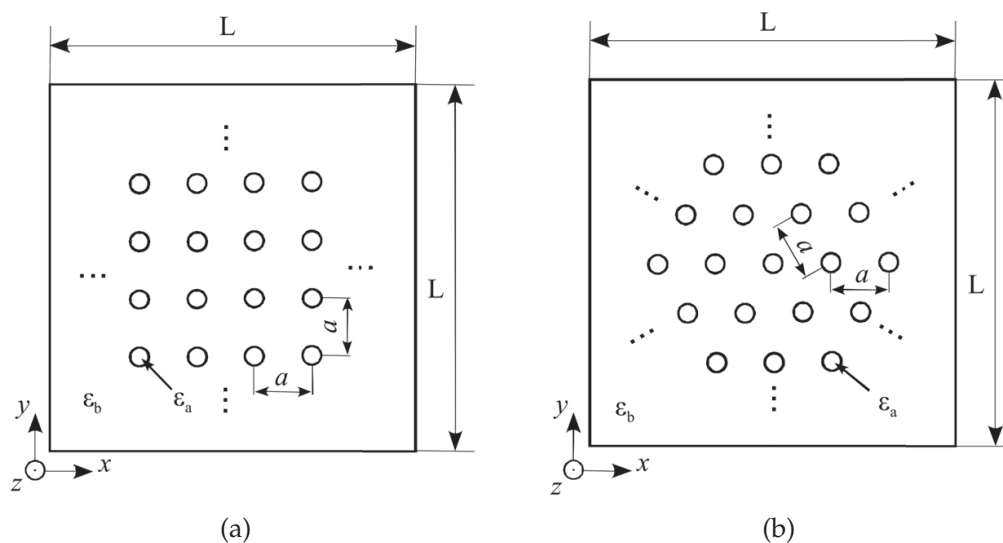

Fig. 1. a) Square and b) triangular lattice photonic structure cross section. (ε_a and ε_b are relative permittivities of rods and background material, respectively, a - lattice constant, L - cavity length)

In crystallography the ideal crystal is described by the elementary cell. The shape of the cell is defined by the basic vectors which linear combination allows to specify the location of all nodes of the structure. Each node is connected to the base which may be constituted by an atom, a group of atoms, molecules, etc. The photonic structures perfectly resemble the microscopic nature of the crystal lattice in the mesoscopic scale. This allows using the terminology adopted in the solid state physics to describe the photonic crystal.

In this chapter, only 2-D photonic crystals will be discussed. In the two-dimensional space, there are five basic types of crystal lattice. This comprises a square, hexagonal, rectangular, oblique, and rhombic lattice (Kittel (1995)). The square and hexagonal (also known as triangular) lattices are the most common types of symmetry used in the practical realizations of photonic cavities. The role of the base in such systems is often played by cylinders called

rods or holes depending on the relative difference between the refractive index of the cylinders and the surrounding material.

The structures in Fig. 1 a) and b) are constrained in the xy plane by the square region of length L, and are assumed to be uniform and much larger than the wavelength in the the z direction. The permittivity of the holes and background material is ε_a and ε_b, respectively. The number of periods in the xy plane is finite, but large enough to be expanded in Fourier series with small error. Schemes in Fig. 1 a) and 1 b) illustrate two spatial distributions of rods for two-dimensional photonic crystal, respectively, with square and triangular lattice.
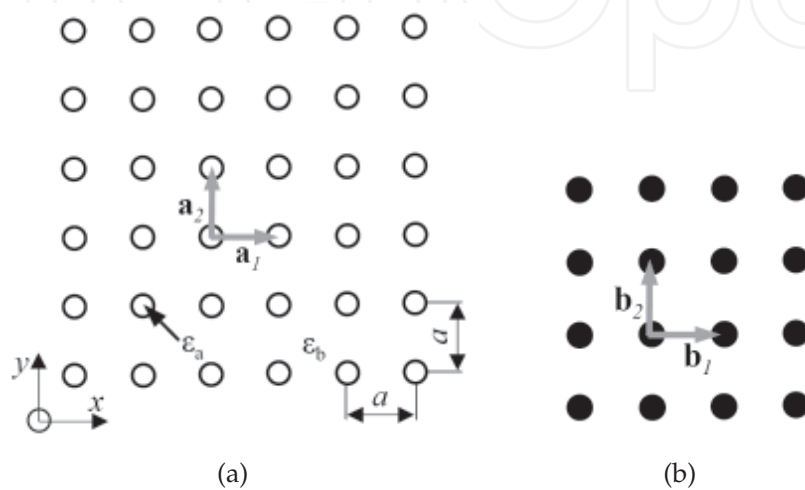

(a)   (b)

Fig. 2. The scheme of a) a square lattice photonic crystal with primitive vectors; and b) its representation in reciprocal space with reciprocal primitive vectors.

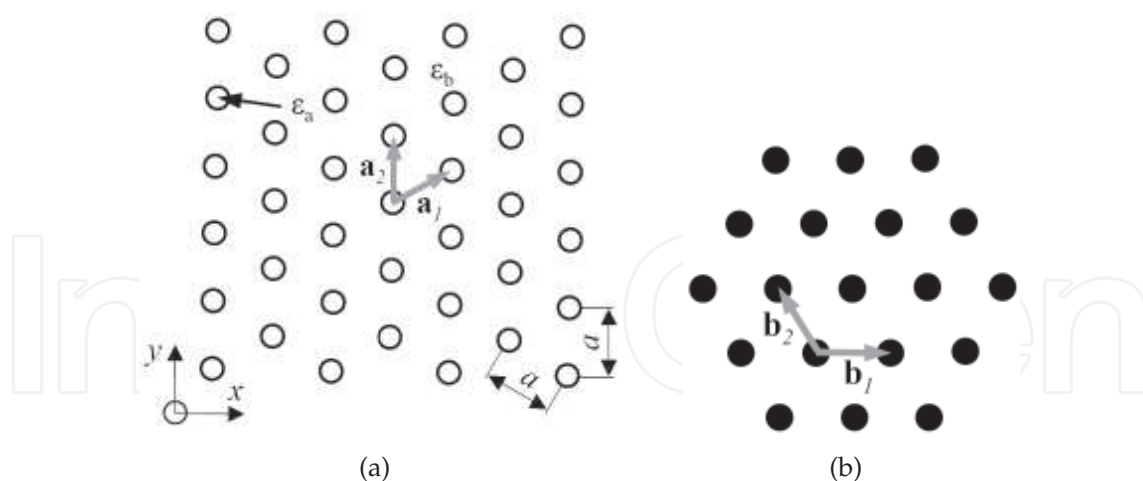(a)   (b)

Fig. 3. The scheme of a) a triangular lattice photonic crystal with primitive vectors; and b) its representation in reciprocal space with reciprocal primitive vectors.

Fig. 2 a) and 3 a) show photonic crystal cross sections in xy plane with cylinders arranged in square or triangular lattice with period a, and with depicted primitive vectors $\mathbf{a}_1$ and $\mathbf{a}_2$.

Fig. 2 b) and 3 b) show the reciprocal lattices corresponding, respectively, to the real square and triangular lattice. In the described case, the nodes of a two-dimensional structure can be

expressed by

$$\mathbf{x}_\parallel (l) = l_1 \mathbf{a}_1 + l_2 \mathbf{a}_2 \tag{1}$$

where $\mathbf{a}_1$ and $\mathbf{a}_2$ are primitive vectors (Kittel (1995)), l_1 and l_2 are arbitrary integers, $\mathbf{x}_\parallel$ specifies the placement on the plane, $\mathbf{x}_\parallel = \hat{\mathbf{x}} x + \hat{\mathbf{y}} y$, where $\hat{\mathbf{x}}$ and $\hat{\mathbf{y}}$ are unit vectors along x and y axis, respectively. The area of primitive cell is $a_c = |\mathbf{a}_1 \times \mathbf{a}_2| = a^2$ in case of square lattice, and $a_c = |\mathbf{a}_1 \times \mathbf{a}_2| = \sqrt{3} a^2 / 2$ in case of triangular lattice. Primitive vectors for square lattice are described by the expressions: $\mathbf{a}_1 = (a, 0)$, $\mathbf{a}_2 = (0, a)$, and for the triangular lattice: $\mathbf{a}_1 = \left(\sqrt{3} a / 2, a / 2 \right)$, $\mathbf{a}_2 = (0, a)$.

In general, the reciprocal vecotrs can be written in the following form:

$$\mathbf{G}(h) = h_1 \mathbf{b}_1 + h_2 \mathbf{b}_2 \tag{2}$$

where h_1 and h_2 are arbitrary integers, $\mathbf{b}_1$ and $\mathbf{b}_2$ are the primitive vectors of the two-dimensional reciprocal lattice:

$$\mathbf{b}_1 = \frac{2\pi}{a_c} \left(a_y^{(2)}, -a_x^{(2)} \right), \qquad \mathbf{b}_2 = \frac{2\pi}{a_c} \left(-a_y^{(1)}, a_x^{(1)} \right), \tag{3}$$

where $a_j^{(i)}$ is the j-th cartesian component (x or y) of the $\mathbf{a}_i$ vector ($i = 1$ lub 2) (Sakai et al. (2010)).

Using Equation 3 and the expressions for square and triangular lattice primitive vectors the reciprocal primitive vectors are described by the following formulas:

$$\mathbf{b}_1 = (2\pi/a, 0), \qquad \mathbf{b}_2 = (0, 2\pi/a) - \text{square lattice} \tag{4}$$

and

$$\mathbf{b}_1 = \left(4\pi/\sqrt{3}a, 0 \right), \qquad \mathbf{b}_2 = \left(-2\pi/\sqrt{3}a, 2\pi/a \right) - \text{triangular lattice.} \tag{5}$$

The infinite square or triangular photonic crystal can be described in terms of relative permittivity by the functions:

$$\varepsilon^{-1} \left(\mathbf{x}_\parallel \right) = \varepsilon_b^{-1} + \left(\varepsilon_a^{-1} - \varepsilon_b^{-1} \right) \sum_l S \left(\mathbf{x}_\parallel - \mathbf{x}_\parallel (l) \right) \tag{6}$$

in case of TE polarization, where it is more convenient to use the inverse of relative permittivity, and

$$\varepsilon \left(\mathbf{x}_\parallel \right) = \varepsilon_b + \left(\varepsilon_a - \varepsilon_b \right) \sum_l S \left(\mathbf{x}_\parallel - \mathbf{x}_\parallel (l) \right) \tag{7}$$

for TM polarization. In previous Equations, function S

$$S \left(x_\parallel \right) = \begin{cases} 1 & \text{dla } \mathbf{x}_\parallel \in O \\ 0 & \text{dla } \mathbf{x}_\parallel \notin O \end{cases} \tag{8}$$

specifies the location of rods in the structure, O is the area of the xy plane defined by the cross section of the rod, which symmetry axis intersects the plane at the point $x_\parallel = 0$.

The functions describing the structure need to be transformed to the frequency domain in order to solve the wave equations. To do so, the crystal geometry is expressed in terms of reciprocal lattice vector by the Fourier transformation of functions 6 and 7 (M. Plihal & Maradudin (1991); M. Plihal et al. (1991)).

For TE polarization function $\epsilon^{-1}(\mathbf{G})$ is written in the following form:

$$\epsilon^{-1}(\mathbf{G}) = \begin{cases} \varepsilon_a^{-1} f + \varepsilon_b^{-1} (1-f), & \mathbf{G}_{\parallel} = 0 \\ \left(\varepsilon_a^{-1} - \varepsilon_b^{-1}\right) f \dfrac{2J_1(\mathbf{G}_{\parallel}R)}{(\mathbf{G}_{\parallel}R)}, & \mathbf{G}_{\parallel} \neq 0 \end{cases} \tag{9}$$

and for the TM polarization function $\epsilon(\mathbf{G})$:

$$\epsilon(\mathbf{G}) = \begin{cases} \varepsilon_a f + \varepsilon_b (1-f), & \mathbf{G}_{\parallel} = 0 \\ (\varepsilon_a - \varepsilon_b) f \dfrac{2J_1(\mathbf{G}_{\parallel}R)}{(\mathbf{G}_{\parallel}R)}, & \mathbf{G}_{\parallel} \neq 0 \end{cases} \tag{10}$$

where $f = \pi r^2/a^2$ – square lattice filling factor, $f = \left(2\pi/\sqrt{3}\right) r^2/a^2$ – triangular lattice filling factor, r – rod radius, J_1 – Bessel function of the first kind.

In further parts of this chapter four different cases have been analyzed. Two of them are dedicated to square lattice cavities with TE and TM polarization, and two remaining to triangular lattice structures also with TE and TM polarization.

In the next parts of this chapter the threshold and above threshold analysis of the photonic crystal laser operation has been shown for the defined structures.

3. A threshold analysis

3.1 Coupled-wave equations

In general, the scalar wave equations for the electric and magnetic fields E_z and H_z, respectively, are written in the following form (M. Plihal & Maradudin (1991); M. Plihal et al. (1991)):

$$\frac{\partial^2 E_z}{\partial x^2} + \frac{\partial^2 E_z}{\partial y^2} + k^2 E_z = 0 \tag{11}$$

and

$$\frac{\partial}{\partial x} \left\{ \frac{1}{k^2} \frac{\partial}{\partial x} H_z \right\} + \frac{\partial}{\partial y} \left\{ \frac{1}{k^2} \frac{\partial}{\partial y} H_z \right\} + H_z = 0 \tag{12}$$

where the constant k is given by (Sakai et al. (2007))

$$k^2 = \beta^2 + 2i (\alpha - \alpha_L) \beta + 2\beta \sum_{\mathbf{G} \neq 0} \kappa(\mathbf{G}) \exp(i(\mathbf{G} \cdot \mathbf{r})) \tag{13}$$

in case of TM modes, and (Sakai et al. (2010))

$$\frac{1}{k^2} = \frac{1}{\beta^4} \left(\beta^2 - i2 \left(\alpha - \alpha_L \right) \beta + 2\beta \sum_{\mathbf{G} \neq 0} \kappa(\mathbf{G}) \exp \left(i \left(\mathbf{G} \cdot \mathbf{r} \right) \right) \right) \qquad (14)$$

in case of TE modes. In Equations 13 and 14 $\beta = 2\pi \varepsilon_0^{1/2} / \lambda$ where $\varepsilon_0 = \varepsilon \left(\mathbf{G} = 0 \right)$ is the averaged dielectric permittivity ($\varepsilon_0^{1/2}$ corresponds to averaged refractive index n), α is an averaged gain in the medium, $\kappa(\mathbf{G})$ is the coupling constant, λ is the Bragg wavelength, and $\mathbf{G} = \left(m\mathbf{b}_1, n\mathbf{b}_2 \right)$ is the reciprocal lattice vector, m and n are arbitrary integers, $\mathbf{b}_1$ and $\mathbf{b}_2$ vary depending on the structure symmetry. Therefore, these vectors are expressed in the following forms $\mathbf{b}_1 = \left(\beta_0^s, 0 \right)$ and $\mathbf{b}_2 = \left(0, \beta_0^s \right)$ for square lattice, and $\mathbf{b}_1 = \left(\beta_0^t, 0 \right)$ and $\mathbf{b}_2 = \left(-\beta_0^t / 2, \sqrt{3}\beta_0^t / 2 \right)$ for triangular lattice structure, where $\beta_0^s = 2\pi / a$ and $\beta_0^t = 4\pi / \sqrt{3}a$. In the derivation of Equations 13 and 14 following e.g. (Sakai et al. (2007)), we set $\alpha \ll \beta \equiv \frac{2\pi \varepsilon_0^{1/2}}{\lambda}$, $\varepsilon_{\mathbf{G} \neq 0} \ll \varepsilon_0$, and $\alpha_{\mathbf{G}} \ll \beta$. In these equations the periodic variation in the refractive index is included as a small perturbation and appears in the third term through the coupling constant $\kappa(\mathbf{G})$ of the form:

$$\kappa(\mathbf{G}) = -\frac{\pi}{\lambda \varepsilon_0^{1/2}} \varepsilon(\mathbf{G}) \pm i \frac{\alpha(\mathbf{G})}{2}. \qquad (15)$$

In Equation 15, plus sign refers to TM polarization (Equation 13), while minus sign refers to TE polarization (Equation 14). Furthermore, we set $\alpha(\mathbf{G})|_{\mathbf{G} \neq 0} = 0$ neglecting spatial periodicity of gain. In the vicinity of the Bragg wavelength only some of the diffraction orders contribute in a significant way, where in general, a periodic perturbation produces an infinite set of diffraction orders. Therefore the Bragg frequency orders have to be cautiously chosen. The Bragg frequency corresponding to the Γ point in the photonic band structure, e.g. (Sakai et al. (2007)) is chosen for the purpose of this paper, and the most significantly contributing coupling constants are expressed as follows:

$$\kappa_1 = \kappa(\mathbf{G})|_{|\mathbf{G}|=\beta_0^{s,t}} \quad \kappa_2 = \kappa(\mathbf{G})|_{|\mathbf{G}|=\sqrt{3}\beta_0^{s,t}} \quad \kappa_3 = \kappa(\mathbf{G})|_{|\mathbf{G}|=2\beta_0^{s,t}} \qquad (16)$$

In Equations 11 and 12 electric and magnetic fields for the infinite periodic structure are given by the Bloch modes, (M. Plihal & Maradudin (1991); Vurgaftman & Meyer (2003)):

$$E_z(\mathbf{r}) = \sum_{\mathbf{G}} e(\mathbf{G}) \exp \left(i \left(\mathbf{k} + \mathbf{G} \right) \cdot \mathbf{r} \right) \qquad (17)$$

and

$$H_z(\mathbf{r}) = \sum_{\mathbf{G}} h(\mathbf{G}) \exp \left(i \left(\mathbf{k} + \mathbf{G} \right) \cdot \mathbf{r} \right) \qquad (18)$$

where the functions $e(\mathbf{G})$ and $h(\mathbf{G})$ correspond to plane wave amplitudes, and the wave vector is denoted by $\mathbf{k}$. In the first Brillouin zone at the Γ point the wave vector vanishes $\mathbf{k} = 0$, see e.g. (Sakai et al. (2006)). For a finite structure, the amplitude of each plane wave is not constant, so $e(\mathbf{G})$ and $h(\mathbf{G})$ become functions of space. At the Γ point we consider only the amplitudes ($e(\mathbf{G})$, $h(\mathbf{G})$) which are meant to be significant, i.e. in most cases with $|\mathbf{G}| = \beta_0^{s,t}$, except for square lattice with TE polarization where additional $h(\mathbf{G})$ amplitudes

with $|\mathbf{G}| = \sqrt{2}\beta_0^s$ have to be included (Sakai et al. (2006)). The contributions of other waves of higher order in the Bloch mode are considered to be negligible.

3.1.1 Square lattice - TM polarization

Considering square lattice photonic crystal with TM polarization, it is assumed that at the Γ point the most significant contribution to coupling is given by the electric waves which fulfill the condition $\left(|\mathbf{G}| = \beta_0^s\right)$. Thus, all higher order electric wave expansion coefficients $\left(|\mathbf{G}| \geq \sqrt{2}\beta_0\right)$ are negligible. Four basic waves most significantly contributing to coupling are depicted in Fig. 4.
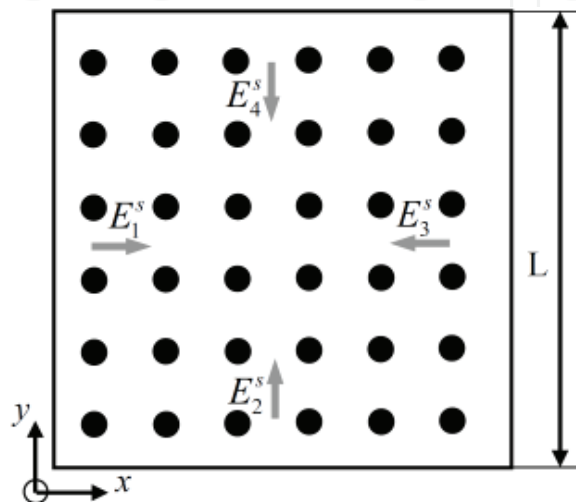
Fig. 4. Schematic cross section of square lattice photonic crystal laser active region, where the four basic waves involved in coupling for TM polarization are shown.

Equation 17 describes infinite structures. It is possible to take into account the fact that the structure is finite by using the space dependent amplitudes, e.g. (Sakai et al. (2007)). Thus, the electric field given by Equation 17 in the finite periodic structure can be expressed in the following way:

$$E_z = E_1^s(x,y)e^{-i\beta_0^s x} + E_2^s(x,y)e^{i\beta_0^s x} + E_3^s(x,y)e^{-i\beta_0^s y} + E_4^s(x,y)e^{i\beta_0^s y} \qquad (19)$$

In Equation 19 E_i^s, $i = 1..4$ are the four basic electric field amplitudes propagating in four directions $+x, -x, +y, y$. These amplitudes correspond to $e(\mathbf{G})$ in Equation 17. In the further analysis, we will drop the space dependence notation.

Knowing the reciprocal lattice vectors for the square lattice PC, the coupling coefficients $\kappa(\mathbf{G})$ 16 can be written as:

$$\kappa_1 = \frac{\pi\left(\varepsilon_a - \varepsilon_b\right)}{a\left(\varepsilon_a f + \varepsilon_b\left(1-f\right)\right)} \frac{2fJ_1\left(2\sqrt{\pi f}\right)}{\left(2\sqrt{\pi f}\right)} \qquad (20)$$

$$\kappa_2 = \frac{\pi\left(\varepsilon_a - \varepsilon_b\right)}{a\left(\varepsilon_a f + \varepsilon_b\left(1-f\right)\right)} \frac{2fJ_1\left(2\sqrt{2\pi f}\right)}{\left(2\sqrt{2\pi f}\right)} \qquad (21)$$

$$\kappa_3 = \frac{\pi\left(\varepsilon_a - \varepsilon_b\right)}{a\left(\varepsilon_a f + \varepsilon_b\left(1-f\right)\right)} \frac{2fJ_1\left(4\sqrt{\pi f}\right)}{\left(4\sqrt{\pi f}\right)} \qquad (22)$$

Putting Equations 13 and 19 into Equation 11, and assuming the slow varying electromagnetic field, one can get the set of coupled mode equations (Sakai et al. (2007)):

$$-\frac{\partial}{\partial x}E_1^s + (\alpha - \alpha_L - \kappa_0 - i\delta)E_1^s = (i\kappa_3 - \kappa_0)E_3^s + i\kappa_2(E_2^s + E_4^s) \tag{23}$$

$$\frac{\partial}{\partial x}E_3^s + (\alpha - \alpha_L - \kappa_0 - i\delta)E_3^s = (i\kappa_3 - \kappa_0)E_1^s + i\kappa_2(E_2^s + E_4^s) \tag{24}$$

$$-\frac{\partial}{\partial y}E_2^s + (\alpha - \alpha_L - \kappa_0 - i\delta)E_2^s = (i\kappa_3 - \kappa_0)E_4^s + i\kappa_2(E_1^s + E_3^s) \tag{25}$$

$$\frac{\partial}{\partial y}E_4^s + (\alpha - \alpha_L - \kappa_0 - i\delta)E_4^s = (i\kappa_3 - \kappa_0)E_2^s + i\kappa_2(E_1^s + E_3^s) \tag{26}$$

where

$$\delta = (\beta^2 - \beta_0^{s2})/2\beta \approx \beta - \beta_0^s \tag{27}$$

is the Bragg frequency deviation, κ_2 and κ_3 are coupling coefficients expressed by Equations 21 and 22 (Sakai et al. (2007)). The κ_2 coefficient is responsible for orthogonal coupling (e.g. the coupling of E_1^s to E_2^s and E_4^s), and κ_2 corresponds to backward coupling (e.g. the coupling of E_1^s to E_3^s). The additional coefficient κ_0 denotes surface emission losses, and it is proportional to κ_1 (Sakai et al. (2007; 2010)). Solution of Equations 23-26 for the boundary conditions:

$$E_1^s(-\frac{L}{2},y) = E_3^s(\frac{L}{2},y) = 0, E_2^s(x,-\frac{L}{2}) = E_4^s(x,\frac{L}{2}) = 0 \tag{28}$$

defines eigenmodes of the photonic structure. The analysis of this solution will be shown in section 3.2.

3.1.2 Square lattice - TE polarization

In the square lattice photonic crystal cavity with TE polarization, as mentioned before, the coupling process involves magnetic waves satisfying following conditions: $(|\mathbf{G}| = \beta_0)$ and $\left(|\mathbf{G}| = \sqrt{2}\beta_0\right)$, (Sakai et al. (2010)), neglecting higher order Bloch modes. Eight basic waves most significantly contributing to coupling are depicted in Fig. 5.

Similarly as in the case of TM polarization, the equation for magnetic field (Equation 18) describes modes for infinite structure. Thus, the finite dimensions of the structure are described by spatial dependence of magnetic field amplitudes (Sakai et al. (2010)), and the magnetic field 18 is written in the following form:

$$H_z(\mathbf{r}) = H_1^s(x,y)e^{-i\beta_0^s x} + H_5^s(x,y)e^{i\beta_0^s x} + H_3^s(x,y)e^{-i\beta_0^s y} + H_7^s(x,y)e^{i\beta_0^s y} + H_2^s(x,y)e^{-i\beta_0^s x - i\beta_0^s y}$$

$$+ H_4^s(x,y)e^{i\beta_0^s x - i\beta_0^s y} + H_6^s(x,y)e^{i\beta_0^s x + i\beta_0^s y} + H_8^s(x,y)e^{-i\beta_0^s x + i\beta_0^s y} \tag{29}$$

In Equation 29 H_i^s, $i = 1..8$ are the eight basic magnetic field amplitudes of waves propagating in directions schematically shown in Fig. 5. These amplitudes correspond to $h(\mathbf{G})$ in Equation 18. Joining Equations 14, 29, and 12, and assuming slowly varying amplitudes, the coupled
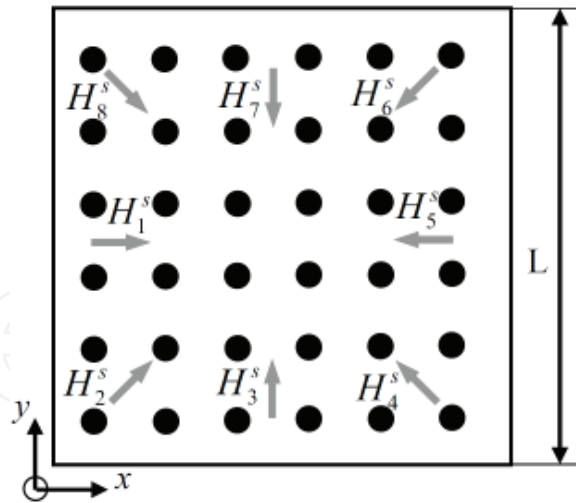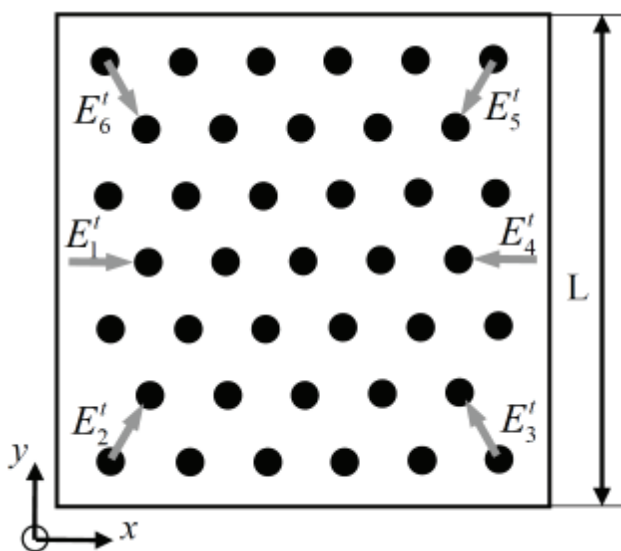
Fig. 5. Schematic cross section of square lattice photonic crystal laser active region, where the eight basic waves involved in coupling for TE polarization are shown.

wave equations for TE modes in square lattice PC are obtained (Sakai et al. (2010)):

$$-\frac{\partial}{\partial x}H_1^s + (\alpha - \alpha_L - \kappa_0 - i\delta)\, H_1^s = (i\kappa_3 - \kappa_0)\, H_5^s + i\frac{2\kappa_1^2}{\beta_0^s}(2H_1^s + H_3^s + H_7^s) \tag{30}$$

$$\frac{\partial}{\partial x}H_5^s + (\alpha - \alpha_L - \kappa_0 - i\delta)\, H_5^s = (i\kappa_3 - \kappa_0)\, H_1^s + i\frac{2\kappa_1^2}{\beta_0^s}(2H_5^s + H_3^s + H_7^s) \tag{31}$$

$$-\frac{\partial}{\partial x}H_3^s + (\alpha - \alpha_L - \kappa_0 - i\delta)\, H_3^s = (i\kappa_3 - \kappa_0)\, H_7^s + i\frac{2\kappa_1^2}{\beta_0^s}(2H_3^s + H_1^s + H_5^s) \tag{32}$$

$$\frac{\partial}{\partial x}H_7^s + (\alpha - \alpha_L - \kappa_0 - i\delta)\, H_7^s = (i\kappa_3 - \kappa_0)\, H_3^s + i\frac{2\kappa_1^2}{\beta_0^s}(2H_7^s + H_1^s + H_5^s) \tag{33}$$

In Equations 30-33, the spatial dependence of H_i^s, $i = 2, 4, 6, 8$ amplitudes was neglected, and it was assumed that $\alpha \ll \delta$. In Equations 30-33, δ is the Bragg frequency deviation, given by 27. The coupling coefficients κ_1, κ_2, and κ_3, defined by Equations 16 are expressed by (Sakai et al. (2010; 2008)):

$$\kappa_1 = \frac{\pi\left(\varepsilon_a^{-1} - \varepsilon_b^{-1}\right)}{a\left(\varepsilon_a^{-1}f + \varepsilon_b^{-1}(1-f)\right)}\frac{2fJ_1\left(2\sqrt{\pi f}\right)}{\left(2\sqrt{\pi f}\right)} \tag{34}$$

$$\kappa_2 = \frac{\pi\left(\varepsilon_a^{-1} - \varepsilon_b^{-1}\right)}{a\left(\varepsilon_a^{-1}f + \varepsilon_b^{-1}(1-f)\right)}\frac{2fJ_1\left(2\sqrt{2\pi f}\right)}{\left(2\sqrt{2\pi f}\right)} \tag{35}$$

$$\kappa_3 = \frac{\pi\left(\varepsilon_a^{-1} - \varepsilon_b^{-1}\right)}{a\left(\varepsilon_a^{-1}f + \varepsilon_b^{-1}(1-f)\right)}\frac{2fJ_1\left(4\sqrt{\pi f}\right)}{\left(4\sqrt{\pi f}\right)} \tag{36}$$

In contrast to TM polarization, in Equations 30-33, the coupling coefficient responsible for coupling in perpendicular direction κ_2 vanishes. The coupling coefficient κ_3 has the same

meaning as described in the previous (TM) case, whereas the coupling coefficient κ_1 describes the coupling of e.g. waves H_1^s, H_2^s, and H_8^s. Solution of Equations 30-33 for the following boundary conditions:

$$H_7^s\left(-\frac{L}{2}, y\right) = H_5^s\left(\frac{L}{2}, y\right) = 0, H_3^s\left(x, -\frac{L}{2}\right) = H_7^s\left(x, \frac{L}{2}\right) = 0 \tag{37}$$

defines structure eigenmodes at lasing threshold i.e. in the linear case.

3.1.3 Triangular lattice - TM polarization

In the triangular lattice photonic crystal cavity with TM polarization, the coupling process involves waves satisfying following conditions ($|\mathbf{G}| = \beta_0$), neglecting higher order Bloch modes (Koba, Szczepanski & Kossek (2011); Sakai et al. (2008)). Six basic waves most significantly contributing to coupling are depicted in Fig. 6.

Fig. 6. A schematic cross section of a triangular lattice photonic crystal laser active region, where the six basic waves involved in the coupling for TM polarization are shown.

The space dependent amplitudes for electric field $e(\mathbf{G})$ (Equation 17) in triangular lattice photonic crystal cavity are written in the following form (Koba, Szczepanski & Kossek (2011)):

$$E_z = E_1^t(x,y)e^{-i\beta_0^t x} + E_2^t(x,y)e^{-i\frac{\beta_0^t}{2}x - i\frac{\sqrt{3}\beta_0^t}{2}y} + E_3^t(x,y)e^{i\frac{\beta_0^t}{2}x - i\frac{\sqrt{3}\beta_0^t}{2}y}$$

$$+ E_4^t(x,y)e^{i\beta_0^t x} + E_5^t(x,y)e^{i\frac{\beta_0^t}{2}x + i\frac{\sqrt{3}\beta_0^t}{2}y} + E_6^t(x,y)e^{-i\frac{\beta_0^t}{2}x + i\frac{\sqrt{3}\beta_0^t}{2}y} \tag{38}$$

In Equation 38, E_i^t, $i = 1..6$, are the six electric field amplitudes propagating in the symmetry directions, Fig. 6. Combining Equations 13, 38 and 11, and assuming slowly varying amplitudes, the coupled wave equations for TM modes in triangular lattice PC are obtained:

$$-\frac{\partial}{\partial x}E_1^t + (\alpha - \alpha_L - \kappa_0 - i\delta)E_1^t = i\kappa_1\left(E_2^t + E_6^t\right) + i\kappa_2\left(E_3^t + E_5^t\right) + (i\kappa_3 - \kappa_0)E_4^t \tag{39}$$

$$-\frac{1}{2}\frac{\partial}{\partial x}E_2^t - \frac{\sqrt{3}}{2}\frac{\partial}{\partial y}E_2^t + (\alpha - \alpha_L - \kappa_0 - i\delta)\,E_2^t =$$
$$= i\kappa_1\left(E_1^t + E_3^t\right) + i\kappa_2\left(E_4^t + E_6^t\right) + (i\kappa_3 - \kappa_0)\,E_5^t \qquad (40)$$

$$\frac{1}{2}\frac{\partial}{\partial x}E_3^t - \frac{\sqrt{3}}{2}\frac{\partial}{\partial y}E_3^t + (\alpha - \alpha_L - \kappa_0 - i\delta)\,E_3^t =$$
$$= i\kappa_1\left(E_2^t + E_4^t\right) + i\kappa_2\left(E_1^t + E_5^t\right) + (i\kappa_3 - \kappa_0)\,E_6^t \qquad (41)$$

$$\frac{\partial}{\partial x}E_4^t + (\alpha - \alpha_L - \kappa_0 - i\delta)E_4^t = i\kappa_1\left(E_3^t + E_5^t\right) + i\kappa_2\left(E_2^t + E_6^t\right) + (i\kappa_3 - \kappa_0)\,E_1^t \qquad (42)$$

$$\frac{1}{2}\frac{\partial}{\partial x}E_5^t + \frac{\sqrt{3}}{2}\frac{\partial}{\partial y}E_5^t + (\alpha - \alpha_L - \kappa_0 - i\delta)\,E_5^t =$$
$$= i\kappa_1\left(E_4^t + E_6^t\right) + i\kappa_2\left(E_1^t + E_3^t\right) + (i\kappa_3 - \kappa_0)\,E_2^t \qquad (43)$$

$$-\frac{1}{2}\frac{\partial}{\partial x}E_6^t + \frac{\sqrt{3}}{2}\frac{\partial}{\partial y}E_6^t + (\alpha - \alpha_L - \kappa_0 - i\delta)\,E_6^t =$$
$$= i\kappa_1\left(E_1^t + E_5^t\right) + i\kappa_2\left(E_2^t + E_4^t\right) + (i\kappa_3 - \kappa_0)\,E_3^t \qquad (44)$$

In Equations 39-44, like in the case of square lattice, δ is the Bragg frequency deviation, given by Equation 27, while κ_1, κ_2, and κ_3 are the coupling coefficients, which are defined by 16 and as follows (Koba, Szczepanski & Kossek (2011)):

$$\kappa_1 = \frac{\pi\,(\varepsilon_a - \varepsilon_b)}{a\,(f\varepsilon_a + (1-f)\,\varepsilon_b)}\frac{2fJ_1(\sqrt{8\pi f/\sqrt{3}})}{\sqrt{8\pi f/\sqrt{3}}} \qquad (45)$$

$$\kappa_2 = \frac{\pi\,(\varepsilon_a - \varepsilon_b)}{a\,(f\varepsilon_a + (1-f)\,\varepsilon_b)}\frac{2fJ_1(\sqrt{\sqrt{3}8\pi f})}{\sqrt{\sqrt{3}8\pi f}} \qquad (46)$$

$$\kappa_3 = \frac{\pi\,(\varepsilon_a - \varepsilon_b)}{a\,(f\varepsilon_a + (1-f)\,\varepsilon_b)}\frac{fJ_1(2\sqrt{8\pi f/\sqrt{3}})}{\sqrt{8\pi f/\sqrt{3}}} \qquad (47)$$

These coefficients describe strength and direction of the coupling of the waves, e.g. the coupling of E_1^t and E_4^t is described by κ_3, the coupling of E_1^t, E_2^t, and E_6^t by κ_1, and the coupling of E_1^t, E_3^t, and E_5^t by κ_2. In Equations 39-44, there is an additional coefficient κ_0 which, like in the square lattice case, is responsible for surface emission losses (Kazarinov & Henry (1985); Vurgaftman & Meyer (2003)). Solution of Equations 39-44 for the boundary conditions:

$$E_1^t(-\frac{L}{2},y) = 0, E_2^t(-\frac{L}{2},y) = E_2^t(x,-\frac{L}{2}) = 0, E_3^t(\frac{L}{2},y) = E_3^t(x,-\frac{L}{2}) = 0,$$
$$E_4^t(\frac{L}{2},y) = 0, E_5^t(\frac{L}{2},y) = E_5^t(x,\frac{L}{2}) = 0, E_6^t(-\frac{L}{2},y) = E_6^t(x,\frac{L}{2}) = 0 \qquad (48)$$

defines structure eigenmodes at lasing threshold.

3.1.4 Triangular lattice - TE polarization

In the triangular lattice photonic crystal cavity with TE polarization, the coupling process involves waves satisfying the same condition as it was stated in TM polarization case, i.e. ($|\mathbf{G}| = \beta_0$), (Sakai et al. (2008)), neglecting higher order Bloch modes. Six basic waves most significantly contributing to coupling are depicted in Fig. 7.
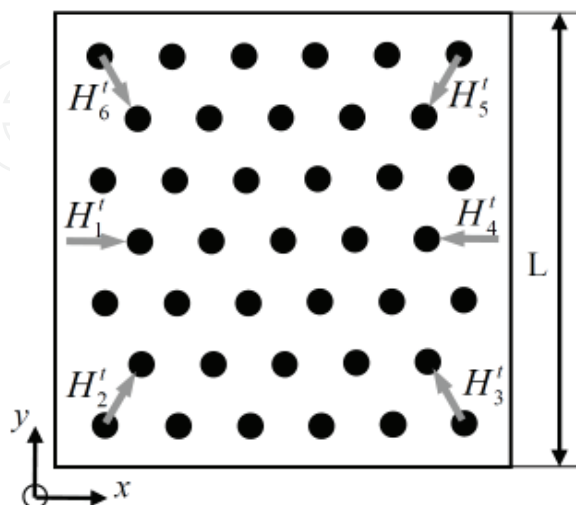

Fig. 7. A schematic cross section of a triangular lattice photonic crystal laser active region, where the six basic waves involved in the coupling for TE polarization are shown.

The magnetic field amplitudes $h(\mathbf{G})$ (Equation 18) in the triangular lattice photonic crystal cavity are written as follows (Sakai et al. (2008)):

$$H_z = H_1^t(x,y)e^{-i\beta_0 x} + H_2^t(x,y)e^{-i\frac{\beta_0}{2}x - i\frac{\sqrt{3}\beta_0}{2}y} + H_3^t(x,y)e^{i\frac{\beta_0}{2}x - i\frac{\sqrt{3}\beta_0}{2}y}$$

$$+ H_4^t(x,y)e^{i\beta_0 x} + H_5^t(x,y)e^{i\frac{\beta_0}{2}x + i\frac{\sqrt{3}\beta_0}{2}y} + H_6^t(x,y)e^{-i\frac{\beta_0}{2}x + i\frac{\sqrt{3}\beta_0}{2}y} \tag{49}$$

In Equation 49, H_i^t, $i = 1..6$, are the six magnetic field amplitudes propagating in the symmetry directions, Fig. 7. Combining Equations 14, 49 and 12, and assuming slowly varying magnetic field amplitudes, the coupled wave equations for TE modes in triangular lattice PC are obtained:

$$-\frac{\partial}{\partial x}H_1^t + (\alpha - \alpha_L - \kappa_0 - i\delta)H_1^t = -i\frac{\kappa_1}{2}\left(H_2^t + H_6^t\right) + i\frac{\kappa_2}{2}\left(H_3^t + H_5^t\right) + (i\kappa_3 - \kappa_0)H_4^t \tag{50}$$

$$-\frac{1}{2}\frac{\partial}{\partial x}H_2^t - \frac{\sqrt{3}}{2}\frac{\partial}{\partial y}H_2^t + (\alpha - \alpha_L - \kappa_0 - i\delta)H_2^t =$$

$$= -i\frac{\kappa_1}{2}\left(H_1^t + H_3^t\right) + i\frac{\kappa_2}{2}\left(H_4^t + H_6^t\right) + (i\kappa_3 - \kappa_0)H_5^t \tag{51}$$

$$\frac{1}{2}\frac{\partial}{\partial x}H_3^t - \frac{\sqrt{3}}{2}\frac{\partial}{\partial y}H_3^t + (\alpha - \alpha_L - \kappa_0 - i\delta)H_3^t =$$

$$= -i\frac{\kappa_1}{2}\left(H_2^t + H_4^t\right) + i\frac{\kappa_2}{2}\left(H_1^t + H_5^t\right) + (i\kappa_3 - \kappa_0)H_6^t \tag{52}$$

$$\frac{\partial}{\partial x}H_4^t + (\alpha - \alpha_L - \kappa_0 - i\delta)H_4^t = -i\frac{\kappa_1}{2}\left(H_3^t + H_5^t\right) + i\frac{\kappa_2}{2}\left(H_2^t + H_6^t\right) + (i\kappa_3 - \kappa_0)H_1^t \tag{53}$$

$$\frac{1}{2}\frac{\partial}{\partial x}H_5^t + \frac{\sqrt{3}}{2}\frac{\partial}{\partial y}H_5^t + (\alpha - \alpha_L - \kappa_0 - i\delta)\,H_5^t =$$

$$= -i\frac{\kappa_1}{2}\left(H_4^t + H_6^t\right) + i\frac{\kappa_2}{2}\left(H_1^t + H_3^t\right) + (i\kappa_3 - \kappa_0)\,H_2^t \tag{54}$$

$$-\frac{1}{2}\frac{\partial}{\partial x}H_6^t + \frac{\sqrt{3}}{2}\frac{\partial}{\partial y}H_6^t + (\alpha - \alpha_L - \kappa_0 - i\delta)\,H_6^t =$$

$$= -i\frac{\kappa_1}{2}\left(H_1^t + H_5^t\right) + i\frac{\kappa_2}{2}\left(H_2^t + H_4^t\right) + (i\kappa_3 - \kappa_0)\,H_3^t \tag{55}$$

where the coupling coefficients κ_1, κ_2, and κ_3 are described by

$$\kappa_1 = \frac{-\pi\left(\varepsilon_a^{-1} - \varepsilon_b^{-1}\right)}{a\left(f\varepsilon_a^{-1} + (1-f)\,\varepsilon_b^{-1}\right)}\frac{2fJ_1(\sqrt{8\pi f/\sqrt{3}})}{\sqrt{8\pi f/\sqrt{3}}} \tag{56}$$

$$\kappa_2 = \frac{-\pi\left(\varepsilon_a^{-1} - \varepsilon_b^{-1}\right)}{a\left(f\varepsilon_a^{-1} + (1-f)\,\varepsilon_b^{-1}\right)}\frac{2fJ_1(\sqrt{8\pi f\sqrt{3}})}{\sqrt{8\pi f\sqrt{3}}} \tag{57}$$

$$\kappa_3 = \frac{-\pi\left(\varepsilon_a^{-1} - \varepsilon_b^{-1}\right)}{a\left(f\varepsilon_a^{-1} + (1-f)\,\varepsilon_b^{-1}\right)}\frac{fJ_1(2\sqrt{8\pi f/\sqrt{3}})}{\sqrt{8\pi f/\sqrt{3}}} \tag{58}$$

and have the same physical meaning like it was described in the TM polarization case. The boundary conditions for the square region of PC with triangular symmetry are written as:

$$H_1^t(-\frac{L}{2}, y) = 0, H_2^t(-\frac{L}{2}, y) = H_2^t(x, -\frac{L}{2}) = 0, H_3^t(\frac{L}{2}, y) = H_3^t(x, -\frac{L}{2}) = 0,$$

$$H_4^t(\frac{L}{2}, y) = 0, H_5^t(\frac{L}{2}, y) = H_5^t(x, \frac{L}{2}) = 0, H_6^t(-\frac{L}{2}, y) = H_6^t(x, \frac{L}{2}) = 0. \tag{59}$$

3.2 Numerical analysis of the PC laser threshold operation

3.2.1 Square lattice - TM and TE polarization

In Fig. 8 enlarged areas of a square lattice photonic crystal dispersion characteristics for the first four modes (A,B,C,D) in the vicinity of Γ point are shown. At the photonic band edge, i.e. at the Γ point, the cavity finesse increases, hence the active medium is used more efficiently. The dispersion curves are plotted for a) TM polarization and b) TE polarization. The plane wave method (Johnson & Joannopoulos (2001)) was used to plot the dispersion characteristic for the infinite two-dimensional PC structure with circular holes $\varepsilon_b = 9.8$ arranged in square lattice with background material $\varepsilon_a = 12.0$. The rods radius to lattice constant ratio was set to 0.24. In each plot, i.e. Fig. 8a) and Fig. 8b), one can observe two degenerate modes: B,C for TM polarization and C,D for TE polarization. They have the same frequency at Γ point. Modes A have the lowest frequency.

In Fig. 8 each of the marked points (A,B,C,D) represents a mode, which is characterized by: Bragg frequency deviation δ, threshold gain α, and threshold field distribution. These characteristic values were calculated by the numerical solution of Equations 23-26 for TM
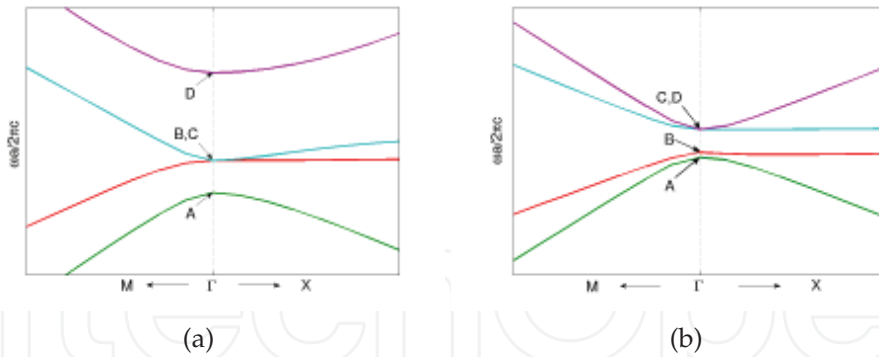
Fig. 8. An enlarged area of a square lattice photonic crystal dispersion curves for the first four modes in the vicinity of Γ point. Square lattice, a) TM polarization, and b) TE polarization.

polarization and Equations 30-33 for TE polarization. In order to assign appropriate points A,B,C,D to the obtained numerical values, it was necessary to use the analytic expressions for the Bragg frequency deviation (Sakai et al. (2006)):

$$\delta_A = -2\kappa_2 - \kappa_3, \quad \delta_{B,C} = \kappa_3, \quad \delta_D = 2\kappa_2 - \kappa_3 \tag{60}$$

in case of TM polarization, and

$$\delta_A = -8\kappa_1^2/\beta_0 - \kappa_3, \quad \delta_B = -\kappa_3, \quad \delta_{C,D} = -4\kappa_1^2/\beta_0 + \kappa_3 \tag{61}$$

in case of TE polarization. These expressions were obtained from Equations 23-26 and 30-33 where no gain ($\alpha = 0$), no loss ($\kappa_0 = 0$, $\alpha_L = 0$), and no spatial dependence of electric or magnetic field amplitude were assumed. Sets of Equations 23-26 and 30-33 were solved numerically for the wide range of coupling coefficients (κ_1, κ_2, κ_3). We grouped obtained solutions: $\left((\delta, \alpha, E_m^s)^j\right)_{\kappa_{3i}}$ or $\left((\delta, \alpha, H_m^s)^j\right)_{\kappa_{3i}}$, where κ_{3i} corresponds to subsequent values of coupling coefficient for different modes $j = A, B, C, D$; $m = 1..4$, s-denotes square lattice. Assigning numerical values of δ_j to analytical solutions 60 and 61 ($\delta_A, \delta_{B,C}, \delta_D$), we obtained the mode structure of 2-D square lattice PC laser with TM and TE polarization.

Fig. 9 and 10 show the field distributions $|\sum_m |E_m^s|^2|$ and $|\sum_m |H_m^s|^2|$, respectively, corresponding to the modes: A - Fig. 9a), D - Fig. 9b), B,C - Fig. 9c), d) for TM modes, and A - Fig. 10a), B - Fig. 10b), C, D - Fig. 10c), d) for TE modes. The plots were made for the normalized coupling coefficients $|\kappa_1 L| = 10.96$, $|\kappa_2 L| = 8$, $|\kappa_3 L| = 4$ and filling factor $f = 0.16$. In each case (TM and TE polarization), the doubly degenerate modes are orthogonal and show saddle-shaped patterns. All non-degenerate modes are similar and exhibit Gaussian-like pattern, and this suggests that these modes should more efficiently use the photonic cavity. These modes also have lower threshold , Fig. 11.

In Fig. 11a) and 11b), the normalized threshold gain αL was plotted as a function of Bragg frequency deviation δL, for various values of the normalized coupling coefficient $|\kappa_3 L|$ (it takes values from 0.01 to 50).

Fig. 11a) and 11b) show that by increasing the value of coupling coefficient the Bragg frequency deviation increases and the threshold gain decreases. Simultaneously, for larger
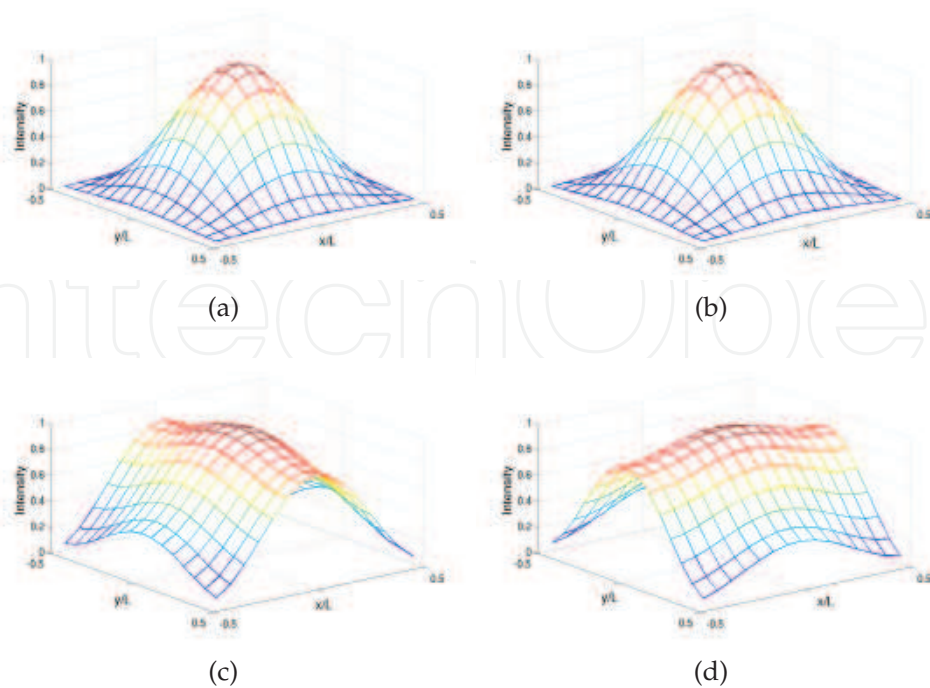
Fig. 9. Electromagnetic field distributions corresponding to a)A, b)D, c)B, and d) C points from Fig. 8a), respectively. Square lattice, TM polarization.
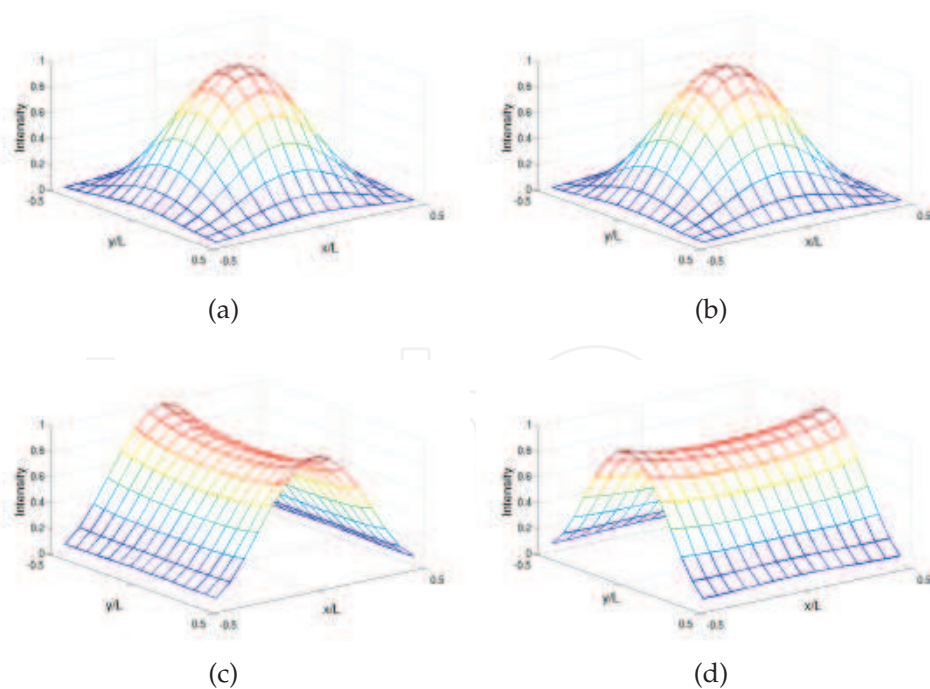

Fig. 10. Electromagnetic field distributions corresponding to a) A, b) B, c) C, and d) D points from Fig. 8b), respectively. Square lattice, TE polarization.

values of coupling coefficient the threshold gain tends to similar values. This tendency is due to growing field confinement in the cavity (all modes become Gaussian-like). In this case the
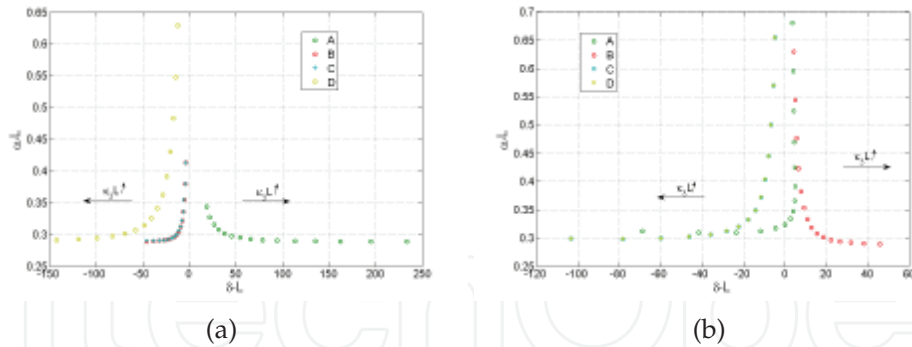
Fig. 11. The dependence of threshold gain versus Bragg frequency deviation. Square lattice, a) TM polarization and b) TE polarization.

mode designation is only possible by the frequency deviation δ. It is also worth noting that the threshold gain values for mode A are the lowest in wide range of coupling coefficient. These modes (A for TM and TE polarization) by having the lowest threshold and by using the active medium in the most efficient way, are favored for lasing.

3.2.2 Triangular lattice - TM and TE polarization

Repeating all the calculations shown for square lattice structures, we obtained threshold characteristics for triangular lattice structures. In Fig. 12 enlarged areas of triangular lattice photonic crystals dispersion curves for the first six modes (A,B,C,D,E,F) in the vicinity of Γ point are shown. Fig. 12a) coresponds to TM polarization, and Fig. 12b) refers to TE polarization. The circular holes $\varepsilon_b = 9.8$ arranged in triangular lattice with background material $\varepsilon_a = 12.0$ were assumed. The rods radius to lattice constant ratio was set to 0.24. In each plot, i.e. Fig. 12a) and Fig. 12b), there can be two pairs of doubly degenerate modes observed: B,C and D,E for TM polarization, and B,C and E,F for TE polarization (they have the same frequency at the Γ point). Modes A have the lowest frequency.

Bragg frequency deviation (for points marked as A,B,C,D,E,F in Fig. 12) depending on coupling coefficient is analytically expressed in the following form for the TM polarization:
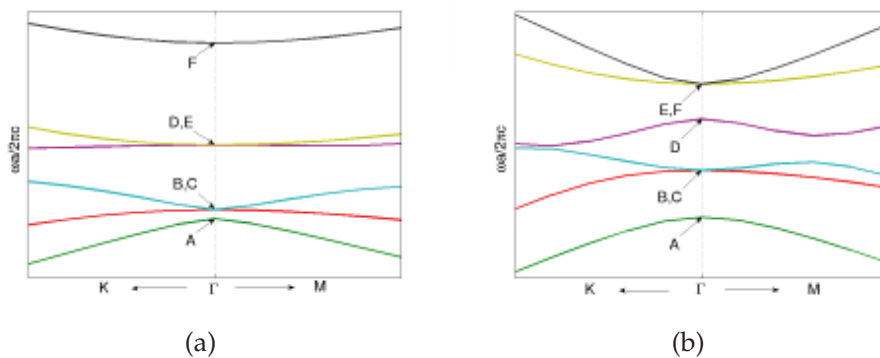

Fig. 12. An enlarged area of dispersion curves of photonic crystal for the first four modes in the vicinity of Γ point. Triangular lattice, a) TM polarization, and b) TE polarization.

$$\delta_A = -2\kappa_1 - 2\kappa_2 - \kappa_3, \quad \delta_{B,C} = -\kappa_1 + \kappa_2 + \kappa_3,$$
$$\delta_{D,E} = \kappa_1 + \kappa_2 - \kappa_3, \quad \delta_F = 2\kappa_1 - 2\kappa_2 + \kappa_3 \tag{62}$$

and for TE polarization:

$$\delta_A = -2\kappa_1 - 2\kappa_2 - \kappa_3, \quad \delta_{B,C} = -\kappa_1 + \kappa_2 + \kappa_3,$$
$$\delta_{D,E} = \kappa_1 + \kappa_2 - \kappa_3, \quad \delta_F = 2\kappa_1 - 2\kappa_2 + \kappa_3. \tag{63}$$

(a)   (b)

(c)   (d)

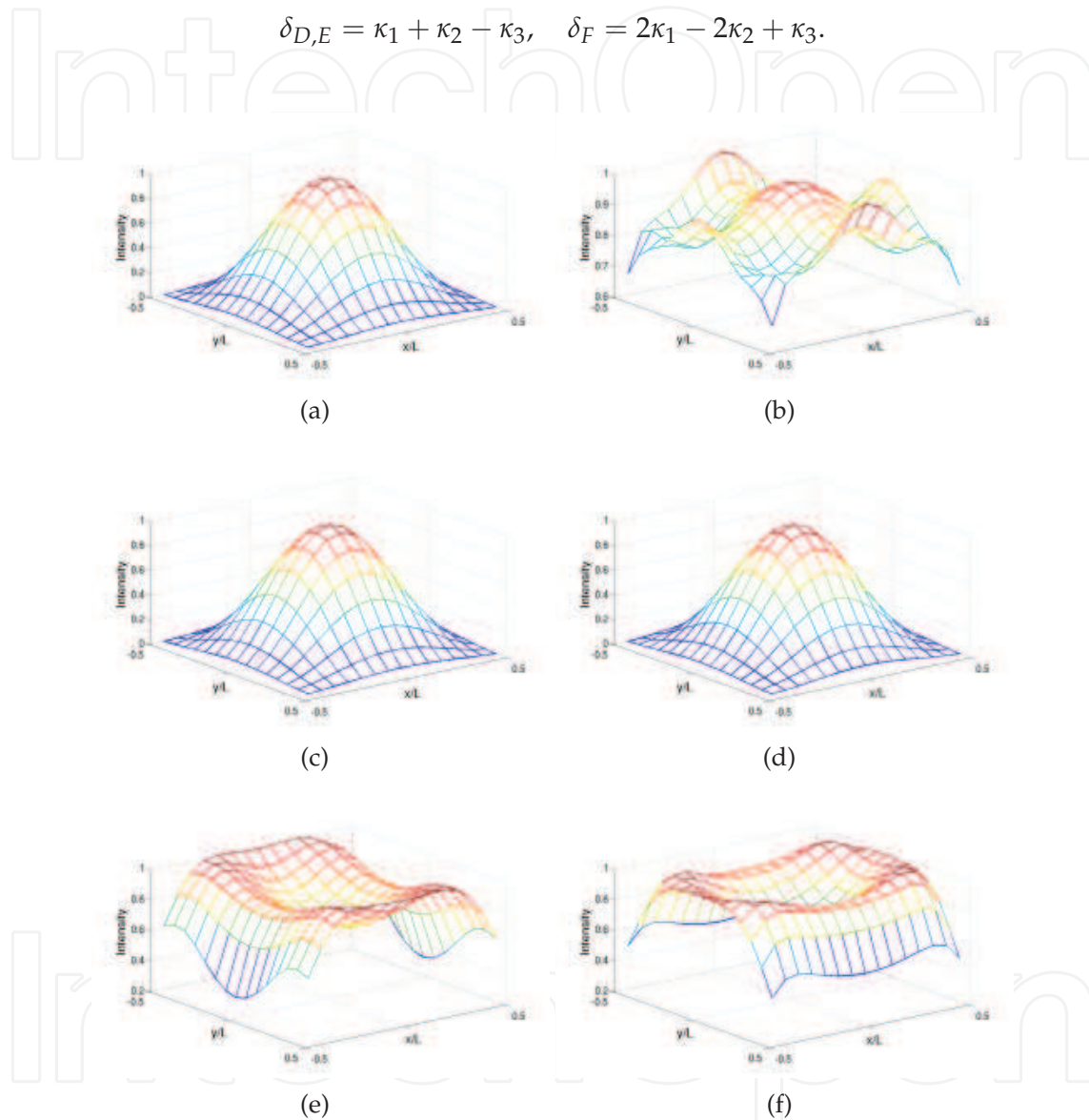(e)   (f)

Fig. 13. Electromagnetic field distributions corresponding to a)A, b)F, c)B, d)C, e)D, and f)E points from Fig. 12a), respectively. Triangular lattice, TM polarization.

Fig. 13 shows the field distributions $|\sum_m |E_m^t|^2|$, $m = 1..6$ corresponding to the modes: A - Fig. 13a), F - Fig. 13b), B,C - Fig. 13c), d), D,E - Fig. 13e), f). Fig. 14 shows the field distributions $|\sum_m |H_m^t|^2|$, $m = 1..6$ corresponding to the modes: A - Fig. 14a), D - Fig. 14b), B,C - Fig. 14c), d), E,F - Fig. 14e), f). We set the values of the normalized coupling coefficients for TM and TE polarization as follows $|\kappa_1 L| = 13.96$, $|\kappa_2 L| = 6.6$, $|\kappa_3 L| = 4$, and the value of the filling factor $f = 0.16$. In case of TM and TE polarization, all degenerate modes are
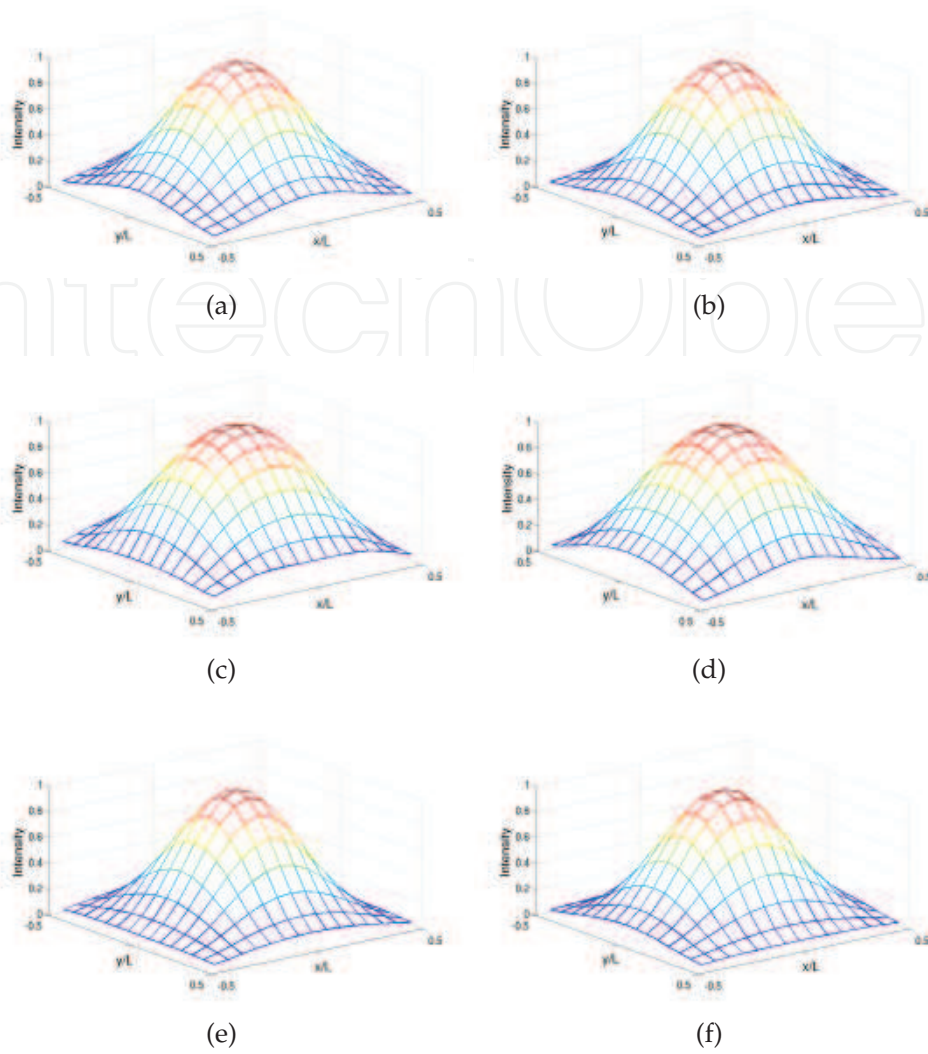
(a)

(b)

(c)

(d)

(e)

(f)

Fig. 14. Electromagnetic field distributions corresponding to a)A, b)D, c)B, d)C, e)E, and f)F points from Fig. 12b), respectively. Triangular lattice, TE polarization.
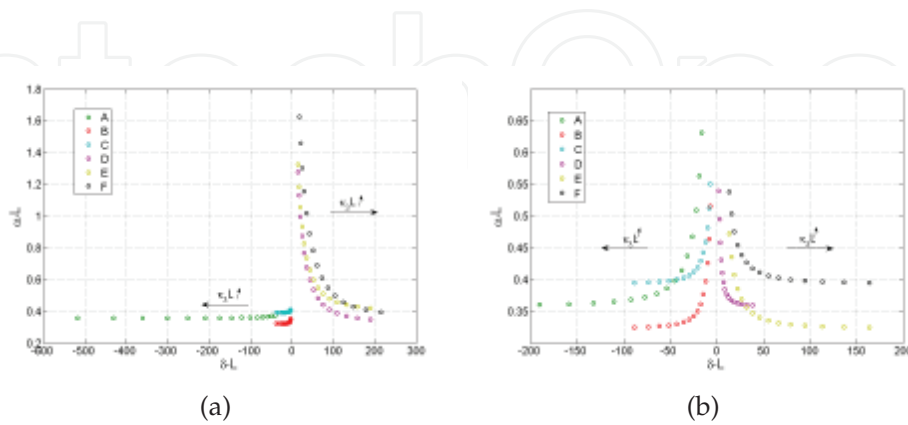

(a)

(b)

Fig. 15. The dependence of threshold gain versus Bragg frequency deviation. Triangular lattice, a) TM polarization, and b) TE polarization.

orthogonal and show similar patterns. For TM polarization, Fig. 13, modes B,C are very similar to the non-degenerate mode A. This means that the coupling coefficients have values for which the modes tend to converge. Similarly for TM polarization, Fig. 14, where two pairs of doubly-degenerate modes are similar to non-degenerate mode A. Likewise, it is due to high values of coupling coefficients and mode convergence.

In Fig. 15a), and 15b) the normalized threshold gain αL was plotted as a function of Bragg frequency deviation δ, for various values of the normalized coupling coefficient $|\kappa_3 L| \in (0.01; 50)$.

Fig. 15 shows similar tendency as in square lattice examples, i.e. by increasing the values of coupling coefficient the Bragg frequency deviation increases and the threshold gain decreases. Simultaneously, for larger values of coupling coefficient the threshold gain tends to similar values. This fact is due to the growing field confinement in the cavity (all modes become Gaussian-like, e.g. Fig. 13 and 14). The mode designation is only possible by obtaining the frequency deviation δ values. The difference in the threshold gain values of degenerate modes stems from numerical inaccuracy, and the threshold gain values should be averaged.

4. An above threshold analysis

The above threshold analysis of light generation in square and triangular lattice two-dimensional photonic crystal laser is based on the energy theorem, presented in e.g. (Koba & Szczepanski (2010)). The introduction of the energy theorem into previously presented coupled wave equations is straightforward but requires laborious calculations. This section presents the results of these calculations, while accurate derivations can be found in (Koba & Szczepanski (2010); Koba, Szczepanski & Kossek (2011); Koba, Szczepanski & Osuch (2011)).

At the basis of the described analysis lies a statement that the energy generated in the structure is equal to the energy leaving the structure and the energy lost in it. In general, the gain coefficient is a function of a small signal gain coefficient α_0, saturation intensity I_S, electric field intensity in the laser structure I, and the shape of gain bandwidth. In the case of a homogenous broadening and the laser action near resonance the gain coefficient is expressed in the following form:

$$\alpha = \frac{\alpha_0}{1 + (I_{in} + \eta I_{coh})/I_S}. \tag{64}$$

In this equation $I_{in} = \sum_i |E_i|^2$ denotes noncoherent component of the electric field, whereas $I_{coh} = \sum_{i \neq j} E_i E_j^*$ is the coherent component, and is responsible for the spatial hole burning effect. The strength of this effect is described by the phenomenological coefficient $\eta \in (0, 1)$.

Equations presented in this section describe the relations between normalized small signal gain coefficient and the laser output power, structure losses, and structure coupling coefficient.

4.1 Square lattice - TM and TE polarization

In order to obtain the expressions describing the small signal gain coefficient in square lattice photonic crystal laser for TM and TE polarization we used the sets of coupled wave Equations 23 - 26 and 30 - 33, (Koba & Szczepanski (2010); Koba, Szczepanski & Osuch (2011)). We added

these sets of equations respectively with their complex conjugates and into each obtained equation we introduced the expression for the nonlinear gain Equation 64. These steps led us to the equations for small signal gain with above threshold field distributions. We replaced the above threshold distributions with the threshold field distributions which we found by numerical solutions of the sets of Equations 23-26 and 30-33. The accuracy of this threshold approximation has been discussed in (Szczepanski (1985)). The final expressions for the small signal gain coefficient of square lattice photonic crystal laser are:

$$\alpha_0 = \left\{ \iint \left(\alpha_L + \kappa_0 \right) M_{th} - 2\kappa_0 \Re \left(T_{th} \right) dxdy + \frac{W_{th}}{2} \right\} \left\{ \iint \frac{M_{th}}{1 + \frac{P_{out}}{P_S} \frac{M_{th} + \eta 2 \Re T_{th}}{W_q}} dxdy \right\}^{-1} \quad (65)$$

where

$$M_{th} = \sum_{m=1}^{4} |E_m^s|^2, \quad T_{th} = E_3^s E_1^{s*} + E_4^s E_2^{s*},$$

and

$$W_{th} = \int_{-L/2}^{L/2} \left| E_1^s \left(\tfrac{L}{2}, y \right) \right|^2 + \left| E_3^s \left(-\tfrac{L}{2}, y \right) \right|^2 dy + \int_{-L/2}^{L/2} \left| E_2^s \left(x, \tfrac{L}{2} \right) \right|^2 + \left| E_4^s \left(x, -\tfrac{L}{2} \right) \right|^2 dx$$

in case of TM polarization, and

$$\alpha_0 = \left\{ \iint \left(\alpha_L + \kappa_0 \right) M_{th} - 2\kappa_0 \Re \left(T_{th} \right) dxdy + \frac{W_{th}}{2} \right\}$$

$$\cdot \left\{ 2 \iint \frac{M_{th}}{1 + \frac{P_{out}}{P_S} \frac{c^2}{(\omega \varepsilon_{av})^2} \frac{\left(M_{th}^{TE} + \eta T_{th}^{TE} \right)}{W_t h}} dxdy \right\}^{-1} \quad (66)$$

where

$$M_{th} = \sum_{m=1}^{4} |H_{2m-1}^s|^2, \quad T_{th} = H_5^s H_1^{s*} + H_7^s H_3^{s*}, \quad M_{th}^{TE} = \sum_{m=1}^{4} \left| \frac{\partial}{\partial x} H_{2m-1}^s \right|^2 + \left| \frac{\partial}{\partial y} H_{2m-1}^s \right|^2,$$

$$W_{th} = \int_{-L/2}^{L/2} \left| H_1^s \left(\tfrac{L}{2}, y \right) \right|^2 + \left| H_5^s \left(-\tfrac{L}{2}, y \right) \right|^2 dy + \int_{-L/2}^{L/2} \left| H_3^s \left(x, \tfrac{L}{2} \right) \right|^2 + \left| H_7^s \left(x, -\tfrac{L}{2} \right) \right|^2 dx,$$

and

$$T_{th}^{TE} = \sum_{\substack{n,m=1 \\ m \neq n}}^{4} \frac{\partial}{\partial x} H_{2m-1}^s \frac{\partial}{\partial x} H_{2n-1}^s + \frac{\partial}{\partial y} H_{2m-1}^s \frac{\partial}{\partial y} H_{2n-1}^s$$

in case of TE polarization. In these equations E_i^t, $i = 1..4$ and H_i^t, $i = 1, 3, 5, 7$ are the electric and magnetic field amplitudes at the lasing threshold (Koba & Szczepanski (2010); Koba, Szczepanski & Osuch (2011)).

4.2 Triangular lattice - TM and TE polarization

Expressions describing the small signal gain coefficients for triangular lattice photonic crystal laser are obtained in the analogical way as we have done for square lattice structure. All necessary calculations can be found in (Koba, Szczepanski & Kossek (2011); Koba, Szczepanski & Osuch (2011)). The starting points for these calculations are Equations 39-44 and 50-55 for TM and TE polarization, respectively. The small signal gain coefficient in triangular lattice photonic crystal laser with TM polarization is described as follows:

$$\alpha_0 = \left\{ \iint (\alpha_L + \kappa_0) M_{th} - 2\kappa_0 \Re \left(E_1^t E_4^{t*} + E_2^t E_5^{t*} + E_3^t E_6^{t*} \right) dxdy + \frac{W_{th}}{2} \right\}$$

$$\cdot \left\{ \iint \frac{M_{th}}{1 + \frac{P_{out}}{P_S} \frac{M_{th} + \eta T_{th}}{W_{th}}} dxdy \right\}^{-1} \tag{67}$$

where

$$M_{th} = \sum_{m=1}^{6} \left| E_m^t \right|^2, \quad T_{th} = \sum_{\substack{m,n=1 \\ m \neq n}}^{6} E_m^t E_n^{t*},$$

and

$$W_{th} = \int_{-L/2}^{L/2} \left[\left| E_1^t \left(\frac{L}{2}, y \right) \right|^2 + \frac{1}{2} \left| E_2^t \left(\frac{L}{2}, y \right) \right|^2 + \frac{1}{2} \left| E_3^t \left(-\frac{L}{2}, y \right) \right|^2 + \left| E_4^t \left(-\frac{L}{2}, y \right) \right|^2 \right.$$

$$\left. + \frac{1}{2} \left| E_5^t \left(-\frac{L}{2}, y \right) \right|^2 + \frac{1}{2} \left| E_6^t \left(\frac{L}{2}, y \right) \right|^2 \right] dy + \frac{\sqrt{3}}{2} \int_{-L/2}^{L/2} \left[\left| E_2^t \left(x, \frac{L}{2} \right) \right|^2 \right.$$

$$\left. + \left| E_3^t \left(x, \frac{L}{2} \right) \right|^2 + \left| E_5^t \left(x, -\frac{L}{2} \right) \right|^2 + \left| E_6^t \left(x, -\frac{L}{2} \right) \right|^2 \right] dx,$$

and for the TE polarization:

$$\alpha_0 = \left\{ \iint (\alpha_L + \kappa_0) M_{th} - 2\kappa_0 \Re \left(H_1^t H_4^{t*} + H_2^t H_5^{t*} + H_3^t H_6^{t*} \right) dxdy + \frac{W_{th}}{2} \right\}$$

$$\cdot \left\{ \iint \frac{M_{th}}{1 + \frac{P_{out}}{P_S} \frac{(c/\omega \varepsilon_{av})^2 \left(M_{th}^{TE} + \eta T_{th}^{TE} \right)}{W_{th}}} dxdy \right\}^{-1} \tag{68}$$

where

$$M_{thq} = \sum_{m=1}^{6} \left| H_m^t \right|^2, \quad M_{thq}^{TE} = \sum_{m=1}^{6} \left| \frac{\partial}{\partial x} H_m^t \right|^2 + \left| \frac{\partial}{\partial y} H_m^t \right|^2,$$

$$T_{th}^{TE} = \sum_{\substack{m,n=1 \\ m \neq n}}^{6} \frac{\partial}{\partial x} H_m^t \frac{\partial}{\partial x} H_n^{t*} + \frac{\partial}{\partial y} H_m^t \frac{\partial}{\partial y} H_n^{t*},$$

and

$$
\begin{aligned}
W_{th} = \int_{-L/2}^{L/2} & \left[\left| H_1^t \left(\tfrac{L}{2}, y \right) \right|^2 + \tfrac{1}{2} \left| H_2^t \left(\tfrac{L}{2}, y \right) \right|^2 + \tfrac{1}{2} \left| H_3^t \left(-\tfrac{L}{2}, y \right) \right|^2 + \left| H_4^t \left(-\tfrac{L}{2}, y \right) \right|^2 \right. \\
& \left. + \tfrac{1}{2} \left| H_5^t \left(-\tfrac{L}{2}, y \right) \right|^2 + \tfrac{1}{2} \left| H_6^t \left(\tfrac{L}{2}, y \right) \right|^2 \right] dy + \tfrac{\sqrt{3}}{2} \int_{-L/2}^{L/2} \left[\left| H_2^t \left(x, \tfrac{L}{2} \right) \right|^2 + \left| H_3^t \left(x, \tfrac{L}{2} \right) \right|^2 \right. \\
& \left. + \left| H_5^t \left(x, -\tfrac{L}{2} \right) \right|^2 + \left| H_6^t \left(x, -\tfrac{L}{2} \right) \right|^2 \right] dx
\end{aligned}
$$

for TE polarization. In Equations 67 and 68 E_i^t, $i = 1..6$ and H_i^t, $i = 1, 3, 5, 7$ are the electric and magnetic field components at the lasing threshold, respectively.

In Equations 65-68, the distinguished factors M_{th}, W_{th}, and T_{th} are associated with total power in the structure, outgoing power, and the spatial hole burning effect. Moreover, in case of TE polarization, an additional factors T_{th}^{TE} and M_{th}^{TE} are included to take into account the electric dipole interaction in terms of magnetic field.

Equations 65-68 allow us to plot the characteristics showing the behavior of small signal gain for different structure parameters.

4.3 Numerical analysis

This section is devoted to the analysis of numerical solutions of Equations 65-68. As mentioned earlier, the field distributions in Equations 65, 66, 67, and 68 are those which exist at lasing threshold. We obtained these threshold field distributions by numerically solving the sets of the coupled equations 23-26, 30-33, 39-44, and 50-55. The presented results describe above threshold operation of square and triangular lattice photonic crystal laser with TM and TE polarization. These results include nonlinear gain, structure imperfections losses, surface emission losses and spatial hole burning effect. In this section we discus modes which are marked as A in Fig. 8 and 12, section 3.
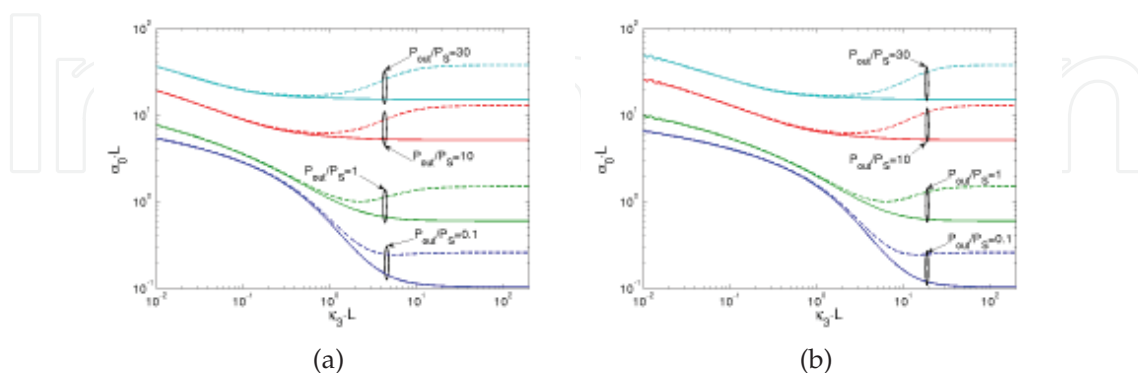

(a)   (b)

Fig. 16. Normalized small signal gain $\alpha_0 L$ vs. the normalized coupling constant $\kappa_3 L$ with the normalized output power level P_{out}/P_S as a parameter, for two values of the normalized losses in the structure, $\alpha_L L = 0$ (solid line) and $\alpha_L L = 0.05$ (dashed line). Surface emission loss $\kappa_0 = 0$. Square lattice photonic crystal structures with a)TM, and b)TE polarization.
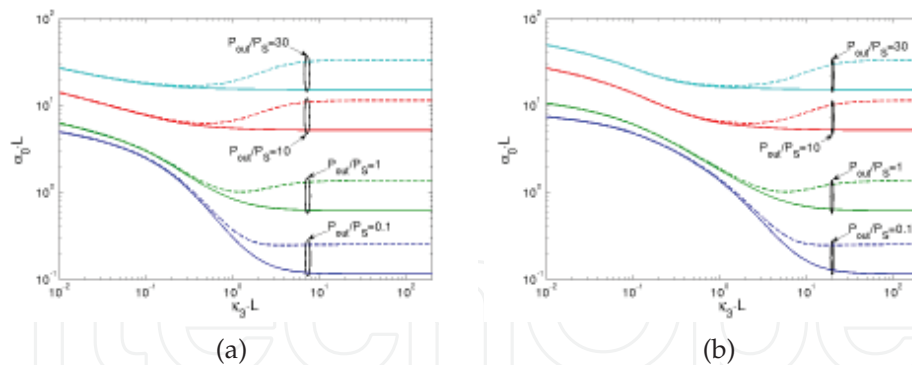
Fig. 17. Normalized small signal gain $\alpha_0 L$ vs. the normalized coupling constant $\kappa_3 L$ with the normalized output power level P_{out}/P_S as a parameter, for two values of the normalized losses in the structure, $\alpha_L L = 0$ (solid line) and $\alpha_L L = 0.05$ (dashed line). Surface emission loss $\kappa_0 = 0$. Triangular lattice photonic crystal structures with a)TM, and b)TE polarization.

Fig. 16 and 17 represent normalized small signal gain coefficient $\alpha_0 L$ as a function of the normalized coupling constant $\kappa_3 L$ with the normalized output power level P_{out}/P_S as a parameter, for two values of the normalized losses in the structure, $\alpha_L L = 0$ (solid line) and $\alpha_L L = 0.05$ (dashed line), respectively.

In case of square lattice, we set the coupling coefficients ratios constant, and they are $\kappa_2/\kappa_3 = 2$ and $\kappa_1/\kappa_3 = 2.74$ (this corresponds to the filling factor $f = 0.16$). Whereas, for triangular lattice we set $\kappa_1/\kappa_3 = 3.49$ and $\kappa_2/\kappa_3 = 1.65$, which is related to the same filling factor as in square lattice case, i.e. $f = 0.16$. Constant ratio of the coupling coefficients corresponds to the situation in which the relative refractive indexes difference vary, but the filling factor remains the same, e.g. Equations 20-22 or 45-47. In the lossless structure with an increasing coupling strength (i.e., increasing Q-factor of the cavity), the small signal gain required to maintain given output power monotonically decreases. This tendency changes, when we introduce losses. In this situation (depicted by dashed lines in Fig. 16 and 17) plotted curves have minima within the considered values of the coupling coefficient $\kappa_3 L$. The minima are caused by nonlinear gain, i.e. the gain saturation effect. Their depth and curve shape depends on the output power P_{out}/P_S, refractive index difference, and filling factor. The minima represent the lowest value of small signal gain for considered system parameters. Thus, for each power level and given other structure parameters, there exists an optimal coupling strength that results in the minimal small signal gain required to maintain that output level. The small signal gain is related to the active medium pumping rate, thus we expect that the pumping level of the laser structure is also minimal. Therefore, we can say that for the optimal coupling strength the laser structure operates at the maximal power efficiency. Moreover, with an increasing output power level, the optimal coupling strength is shifted towards lower values (Koba & Szczepanski (2010); Koba, Szczepanski & Kossek (2011); Koba, Szczepanski & Osuch (2011)).

5. Perspectives

Here, we point out a interesting path for further investigation of photonic crystal lasers. In this chapter we discussed 2-D PC lasers, but since a lot of publications on three-dimensional (3-D)

coupled mode theory are issued e.g.(Hamam et al. (2007)) and 3-D photonic crystal lasers are developed e.g. (Tandaechanurat et al. (2011)) it would be interesting to introduce this 3-D theory to PC lasers. This formulation would have to face some important issues, e.g. the estimation of the number of coupling waves, and increasing number of coupled equations, but it would give a crucial insight into 3-D photonic cavities.

6. Conclusions

In our work we have presented the systematic studies on the threshold and above threshold two-dimensional photonic crystal laser operation. We have shown the comprehensive coupled mode description of photonic crystal laser threshold operation, completing the works of Sakai et al. by presenting the threshold model for triangular lattice structure with TM polarization. Moreover, we conducted our calculations in the wide range of coupling coefficient for all four cases (square and triangular lattice with TM and TE polarization), which also has not yet been done. In addition, we have presented an approximate method of the above threshold analysis of a 2-D photonic crystal laser operation. We showed the approximate formulas for the small signal gain coefficients as a function of system parameters. Furthermore, we made necessary calculations to obtain above threshold characteristics, which depicted that it is possible to attain the optimal coupling strength providing maximal power efficiency of a given 2-D photonic laser structure. We believe that our analysis and methods could be useful in supporting the design process of a laser structure and help understand the principles of photonic crystal band-edge laser operation.

7. References

Asano, T., Song, B.-S. & Noda, S. (2006). Analysis of the experimental Q factors ($\sim$1 million) of photonic crystal nanocavities, *Opt. Express* 14(5): 1996–2002.

Chassagneux, Y., Colombelli, R., Maineult, W., Barbieri, S., Beere, H., Ritchie, D., Khanna, S., Linfield, E. & Davies, A. (2009). Electrically pumped photonic-crystal terahertz lasers controlled by boundary conditions, *Nature* 457: 174–178.

Cojocaru, C., Raineri, F., Raj, R., Monnier, P., Drisse, O., Legouezigou, L., Chandouineau, J.-P., Pommereau, F., Duan, G.-H. & Levenson, A. (2005). Room-temperature simultaneous in-plane and vertical laser operation in a deep-etched inp-based two-dimensional (2d) photonic crystal, *Optoelectronics, IEE Proceedings* - 152(2): 86–89.

Czuma, P. & Szczepanski, P. (2005). Analytical model of one-dimensional SiO_2:Er-doped photonic crystal Fabry-Perot laser: semiclassical approach, Vol. 5723, SPIE, pp. 307–315.

Dunbar, L., Moreau, V., Ferrini, R., Houdré, R., Sirigu, L., Scalari, G., Giovannini, M., Hoyler, N. & Faist, J. (2005). Design, fabrication and optical characterization of quantum cascade lasers at terahertz frequencies using photonic crystal reflectors, *Opt. Express* 13(22): 8960–8968.

Florescu, L., Busch, K. & John, S. (2002). Semiclassical theory of lasing in photonic crystals, *J. Opt. Soc. Am. B* 19(9): 2215–2223.

Hamam, R., Karalis, A., Joannopoulos, J. & Soljacic, M. (2007). Coupled-mode theory for general free-space resonant scattering of waves, *Phys. Rev. A* 75: 053801.

Imada, M., Chutinan, A., Noda, S. & Mochizuki, M. (2002). Multidirectionally distributed feedback photonic crystal lasers, *Phys. Rev. B* 65(19): 195306.

Iwahashi, S., Liang, Y., Sakai, K., Miyai, E., Kunishi, W., Ohnishi, D., Noda, S. & Kurosaka, Y. (2010). On-chip beam-steering photonic-crystal lasers, *Nature Photonics* 4(7): 447–450.

John, S. (1987). Strong localization of photons in certain disordered dielectric superlattices, *Physical Review Letters* 58(23): 2486–2489.

Johnson, S. & Joannopoulos, J. (2001). Block-iterative frequency-domain methods for maxwell's equations in a planewave basis, *Opt. Express* 8(3): 173–190.

Kazarinov, R. & Henry, C. (1985). Second-order distributed feedback lasers with mode selection provided by first-order radiation losses, *Quantum Electronics, IEEE Journal of* 21(2): 144–150.

Kim, M., Kim, C., Bewley, W., Lindle, J., Canedy, C., Vurgaftman, I. & Meyer, J. (2006). Surface-emitting photonic-crystal distributed-feedback laser for the midinfrared, *Applied Physics Letters* 88(19): 191105 –191105–3.

Kittel, C. (1995). *Introduction to Solid State Physics*, Vol. 2011, John Wiley & Sons.

Koba, M. & Szczepanski, P. (2010). Approximate analysis of nonlinear operation of square lattice photonic crystal laser, *Quantum Electronics, IEEE Journal of* 46(6): 1003–1008.

Koba, M., Szczepanski, P. & Kossek, T. (2011). Nonlinear operation of a 2-D triangular lattice photonic crystal laser, *Quantum Electronics, IEEE Journal of* 47(1): 13–19.

Koba, M., Szczepanski, P. & Osuch, T. (2011). Nonlinear analysis of photonic crystal laser, *Journal of Modern Optics* 0(0): 1–13. to be published.

Lee, K.-H., Baek, J.-H., Hwang, I.-K., Lee, Y.-H., Lee, G.-H., Ser, J.-H., Kim, H.-D. & Shin, H.-E. (2004). Square-lattice photonic-crystal vertical-cavity surface-emitting lasers, *Opt. Express* 12(17): 4136–4143.

Lesniewska-Matys, K., Mossakowska-Wyszynska, A. & Szczepanski, P. (2005). Nonlinear operation of planar waveguide laser with photonic crystal, *Physica Scripta* 2005(T118): 107.

Lu, T., Chen, S., Lin, L., Kao, T., Kao, C., Yu, P., Kuo, H., Wang, S. & Fan, S. (2008). GaN-based two-dimensional surface-emitting photonic crystal lasers with AlN/GaN distributed bragg reflector, *Applied Physics Letters* 92(1): 011129 –011129–3.

M. Plihal & Maradudin, A. (1991). Photonic band structure of two-dimensional systems: The triangular lattice, *Phys. Rev. B* 44(16): 8565–8571.

M. Plihal, Shambrook, A., Maradudin, A. & Sheng, P. (1991). Two-dimensional photonic band structures, *Optics Communications* 80(3-4): 199–204.

Matsubara, H., Yoshimoto, S., Saito, H., Jianglin, Y., Tanaka, Y. & Noda, S. (2008). GaN photonic crystal surface-emitting laser at blue-violet wavelengths, *Science* 319(5862): 445–447.

Miyai, E., Sakai, K., Okano, T., Kunishi, W., Ohnishi, D. & Noda, S. (2006). Photonics: Lasers producing tailored beams, *Nature* 441: 946.

Monat, C., Seassal, C., Letartre, X., Viktorovitch, P., Regreny, P., Gendry, M., Rojo-Romeo, P., Hollinger, G., Jalaguier, E., Pocas, S. & Aspar, B. (2001). Inp 2d photonic crystal microlasers on silicon wafer: room temperature operation at 1.55 μm, *Electronics Letters* 37(12): 764–766.

Noda, S. & Yokoyama, M. (2005). Finite-difference time-domain simulation of two-dimensional photonic crystal surface-emitting laser, *Opt. Express* 13(8): 2869–2880.

Nomura, M., Iwamoto, S., Kumagai, N. & Arakawa, Y. (2008). Ultra-low threshold photonic crystal nanocavity laser, *Physica E: Low-dimensional Systems and Nanostructures* 40(6): 1800–1803. 13th International Conference on Modulated Semiconductor Structures.

Sakai, K., Miyai, E. & Noda, S. (2006). Coupled-wave model for square-lattice two-dimensional photonic crystal with transverse-electric-like mode, *Applied Physics Letters* 89(2): 021101–021101–3.

Sakai, K., Miyai, E. & Noda, S. (2007). Two-dimensional coupled wave theory for square-lattice photonic-crystal lasers with tm-polarization, *Opt. Express* 15(7): 3981–3990.

Sakai, K., Miyai, E. & Noda, S. (2010). Coupled-wave theory for square-lattice photonic crystal lasers with te polarization, *Quantum Electronics, IEEE Journal of* 46(5): 788–795.

Sakai, K., Miyai, E., Sakaguchi, T., Ohnishi, D., Okano, T. & Noda, S. (2005). Lasing band-edge identification for a surface-emitting photonic crystal laser, *Selected Areas in Communications, IEEE Journal on* 23(7): 1335–1340.

Sakai, K., Yue, J. & Noda, S. (2008). Coupled-wave model for triangular-lattice photonic crystal with transverse electric polarization, *Opt. Express* 16(9): 6033–6040.

Scherer, H., Gollub, D., Kamp, M. & Forchel, A. (2005). Tunable gainnas lasers with photonic crystal mirrors, *Photonics Technology Letters, IEEE* 17(11): 2247–2249.

Sirigu, L., Terazzi, R., Amanti, M., Giovannini, M., Faist, J., Dunbar, L. & Houdré, R. (2008). Terahertz quantum cascade lasersbased on two-dimensional photoniccrystal resonators, *Opt. Express* 16(8): 5206–5217.

Steinberg, B. & Boag, A. (2006). Propagation in photonic crystal coupled-cavity waveguides with discontinuities in their optical properties, *J. Opt. Soc. Am. B* 23(7): 1442–1450.

Strutt, J. L. R. (1887). On the maintenance of vibrations by forces of double frequency, and on the propagation of waves through a medium endowed with periodic structure, *Philosophical Magazine* 24: 145–159.

Susa, N. (2001). Threshold gain and gain-enhancement due to distributed-feedback in two-dimensional photonic-crystal lasers, *Journal of Applied Physics* 89(2): 815–823.

Szczepanski, P. (1985). Approximate analysis of nonlinear operation of a distributed feedback laser, *Appl. Opt.* 24(21): 3574–3578.

Tandaechanurat, A., Ishida, S., Guimard, D., Nomura, M., Iwamoto, S. & Arakawa, Y. (2011). Lasing oscillation in a three-dimensional photonic crystal nanocavity with a complete bandgap, *Nat Photon* 5: 91–94.

Turnbull, G., Andrew, P., Barnes, W. & Samuel, I. (2003). Operating characteristics of a semiconducting polymer laser pumped by a microchip laser, *Applied Physics Letters* 82(3): 313–315.

Vurgaftman, I. & Meyer, J. (2003). Design optimization for high-brightness surface-emitting photonic-crystal distributed-feedback lasers, *Quantum Electronics, IEEE Journal of* 39(6): 689–700.

Watanabe, H. & Baba, T. (2006). Active/passive-integrated photonic crystal slab mu;-laser, *Electronics Letters* 42(12): 695–696.

Yablonovitch, E. (1987). Inhibited spontaneous emission in solid-state physics and electronics, *Physical Review Letters* 58(20): 2059–2062.

Yablonovitch, E. (1993). Photonic band-gap crystals, *Journal of Physics: Condensed Matter* 5(16): 2443–2460.

Zhang, Z., Yoshie, T., Zhu, X., Xu, J. & Scherer, A. (2006). Visible two-dimensional photonic crystal slab laser, *Applied Physics Letters* 89(7): 071102 –071102–3.
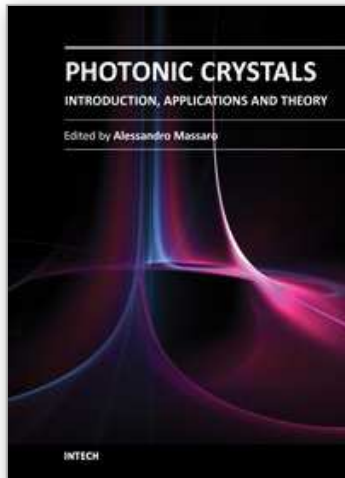
Photonic Crystals - Introduction, Applications and Theory

Edited by Dr. Alessandro Massaro

The first volume of the book concerns the introduction of photonic crystals and applications including design and modeling aspects. Photonic crystals are attractive optical materials for controlling and manipulating the flow of light. In particular, photonic crystals are of great interest for both fundamental and applied research, and the two dimensional ones are beginning to find commercial applications such as optical logic devices, micro electro-mechanical systems (MEMS), sensors. The first commercial products involving two-dimensionally periodic photonic crystals are already available in the form of photonic-crystal fibers, which use a microscale structure to confine light with radically different characteristics compared to conventional optical fiber for applications in nonlinear devices and guiding wavelengths. The goal of the first volume is to provide an overview about the listed issues.

How to reference

In order to correctly reference this scholarly work, feel free to copy and paste the following:

INTECH
open science | open minds